NATIONAL ADVISORY COMMITTEE FOR AERONAUTICS

TECHNICAL NOTE

NO. 1622

ANALYSIS AND PRELIMINARY DESIGN OF AN OPTICAL INSTRUMENT FOR THE MEASUREMENT OF DROP SIZE AND FREE-WATER CONTENT OF CLOUDS

By Willem V. R. Malkus, Richard H. Bishop, and Robert O. Briggs

Ames Aeronautical Laboratory
Moffett Field, Calif.

WASHINGTON
JUNE 1948

NATIONAL ADVISORY COMMITTEE FOR AERONAUTICS

TECHNICAL NOTE NO. 1622

ANALYSIS AND PRELIMINARY DESIGN OF AN OPTICAL INSTRUMENT FOR THE MEASUREMENT OF DROP SIZE AND FREE-WATER CONTENT OF CLOUDS

By Willem V. R. Malkus, Richard H. Bishop
and Robert O. Briggs

SUMMARY

This paper describes a method for the determination of drop size and free water in clouds, based on the interpretation of an artificially created rainbow. Details of the design and operation of an optical instrument employing this method are presented. This instrument is a preliminary design in that the water content and drop size must be kept constant during the interval of the measurement. In designing the instrument, an amplifier which eliminates interference due to shot effect was developed. A mathematical analysis of the rainbow theory is presented in the appendix.

INTRODUCTION

Aircraft icing investigations have necessitated a more complete knowledge of the structure and occurrence of clouds conducive to icing. Various groups in this country and abroad have established stations and developed techniques for this study. Usual methods for measuring the free-water content and average drop size of a cloud have employed rotating cylinders, porous plugs, soot slides, vaseline slides, microphotographs, and differential dew points. While the rotating-cylinder method (reference 1) has been generally regarded as the most accurate and reliable for use in flight, it requires cumbersome projections in the air stream, frequent attention by the observer, and gives results only from an average sample collected during a period of one or two minutes, and only during freezing conditions. The other instruments mentioned, although useful on the ground, have objectionable features for flight operation, for no single device combines such necessities as accuracy, reliability, ease of use, and ability to take frequent readings. Frequency of sampling is important for flight work because local conditions may

change rapidly in traversing a cloud.

In November 1944, research work was initiated by the National Advisory Committee for Aeronautics to devise a method of drop size and free-water determination suited to flight operation. An optical mechanism was thought to offer the best prospects, because it would not require disturbing the air sample. Two optical phenomena were considered: the rainbow and the corona. Practical difficulties of designing an instrument utilizing the corona shifted attention to the less intense rainbow phenomenon. An optical instrument based on rainbow theory has been designed and constructed which offers convenient operation by the observer, no disturbance of air sample, and ability to take very frequent readings (as often as once a second or oftener). Moreover, with this type of instrument, water in the form of liquid drops should be readily distinguishable from snow, sleet, or vapor — a particular advantage for icing investigations; and the instrument is equally usable at temperatures above or below freezing.

The following discussion will consider first the general aspects and principles of the rainbow and its use for measuring drop size and water content, followed by a mathematical analysis of the rainbow and basic recorder characteristics, details of recorder design, and operating experience.

SYMBOLS

The following is a list of the most frequently used symbols:

a	drop radius, microns
B_1	intensity of first maximum
B_2	intensity of second maximum
D	diameter of viewing lens
d	drop diameter
dM	increment of area of wave surface
g	angle of incidence
H	distance from mirror perpendicular to beam
h	distance from mirror to slit
I_B	intensity of beam

I_p	intensity of light from a single drop
I_s	light intensity at dM
K_p	intensity factor
k	distribution, range
L	wave length, microns
n_d	number of droplets in a unit volume
p	angle of viewing
q	angle of refraction
Q^2	intensity factor at wave surface
r_M	distance from mirror to lens
U	horizontal field of view
u	horizontal width of viewing slit
V	vertical field of view
W_B	spectrally effective watts in incident light beam
W_p	total radiation received by slit
w	water content of air, grams per cubic meter
γ	constant phase line
Δ	angle between first two intensity maxima
δ	angle of divergence
σ	constant phase surface

QUALITATIVE DESCRIPTION OF THE RAINBOW

The common rainbow is a multicolored arc seen in rain when the sun is behind the observer; it is a result of reflection, refraction, and interference of sunlight by individual raindrops. The most conspicuous feature of a rainbow is its spectrum of colors, due mainly to differences in the index of refraction of water for different

wavelengths of light. When a rainbow is very bright, one or more subsidiary or "supernumerary" bows may be seen below the first or primary bow; that is, the top (red) band of the second bow starts immediately under the bottom (violet) band of the primary. Usually, only the red band of a supernumerary bow may be seen clearly, but under favorable conditions as many as two supernumeraries may be seen, each with a more or less complete spectrum of colors. If monochromatic light were incident on the cloud instead of white sunlight, there would be a single bright arc in the position of the primary rainbow, with a less bright arc in the position of each supernumerary bow; that is, there would be alternate bright and dark bands. These bands are caused by interference of light waves from different parts of each separate raindrop. It is these alternate bright and dark bands formed by monochromatic light which are of use in measuring drop size and free-water content.

The pattern of rays reflected by a single sphere of water which scatters a beam of parallel monochromatic light is shown (in cross section) in figure 1. The picture in three dimensions may be visualized by rotating the cross section through 360° about the x-axis. The cusped line in figure 1 represents a locus of constant phase. By Fresnel's principle, any two small regions of this wave front may be considered as coherent light sources capable of mutual interference. The total effect at a distant point must be obtained by integration over the entire surface of constant phase. When viewed at a distance, the integrated effect of this mutual interference appears as alternate maxima and minima of intensity. Figure 2 shows the manner in which the intensity varies with viewing angle and also the effect of drop size upon the angular spacing between successive intensity maxima, that is, between bright bands. The angle of viewing p is between the direction of the incident light and the line from the point of observation to the drop.

When more than one particle is observed, corresponding intensities at the point of observation are added arithmetically. For example, five drops all of the same size will give a pattern of the same shape as a single drop, but five times as bright. If the drops are of mixed sizes, bright and dark bands from the various drops will shift in spacing and in angular position, causing partial overlapping of intensity maxima from one group with minima from another group, thus reducing the contrast between bright and dark bands in the overall pattern which results from addition of the separate patterns. Figure 3 shows a typical light intensity distribution pattern for mixed drops. In spite of the reduced contrast, the spacing will still give an accurate indication of the predominant drop size, and the sharpness of the bands is an indication of narrowness in the drop-size distribution range. Thus a single recorded curve showing variation of light intensity with viewing angle contains information as to liquid-water content, average drop size, and range of drop sizes (drop spectrum).

The rainbow should not be confused with corona effects which appear on the far side of a drop, nearly in line with the light source; the corona is due principally to a diffraction effect which bends some of the light rays a few degrees at the edge of the geometric shadow of a fog particle.

GENERAL DESCRIPTION OF RAINBOW INSTRUMENTS

The simplest means of recording a rainbow would be to use an ordinary camera aimed in the proper direction. A collimated light beam would create the rainbow when monochromatic light is used. The resulting light and dark bands on the film can then be measured for density and angular spacing between bands. An important objection to this method is the difficulty of making accurate brightness measurements from the recorded film density. Exposure time, too, is a limitation, even with the most powerful light sources and the most sensitive film. The principal objection is the impossibility of use during daylight hours, for even a small amount of background illumination will darken the film negative sufficiently to make rainbow intensities imperceptible.

It is possible to discriminate between rainbow and background light if the artificial light source used to produce the rainbow is modulated at some chosen frequency, and a detector is used which can discriminate between steady background light and the pulsating light of the rainbow. Direct recording on photographic film is useless for this purpose, since there is no way to determine whether a given film darkening is due to steady or pulsating light. However, if the light is made to fall upon a photoelectric cell, appropriate electrical circuits can readily separate the pulsating component from the steady component and furnish a d-c. output proportional to the intensity of the modulated light. By exposing the photocell successively to small portions of the angular range covered by the rainbow, a record of light intensity distribution as a function of viewing angle may be obtained.

The general arrangement of such an instrument is illustrated in figure 4. A collimated beam of modulated light from light source (A), projected into the air stream, creates the rainbow. An angular increment of the rainbow is seen through a viewing lens (B) and slit (C) by a photocell (D) the current output of which is proportional to the average intensity of that increment. An oscillating mirror (E) allows the photocell to scan successive angular increments of the rainbow during each cycle of motion. A sliding shutter (H), synchronized with the oscillating mirror, cuts off the rainbow during the reverse half of each cycle and simultaneously permits entry of light reflected through two small holes by the two standardization mirrors (F) and (G).

A special cam turns the mirror at constant angular velocity during the forward (rainbow) half of each cycle, thus changing the angle of viewing p at a uniform rate. Hence, a recording galvanometer having deflection proportional to photocell current and having uniform film speed will generate a curve representing rainbow intensity as a function of viewing angle.

Rainbow theory furnishes means for deducing drop size and free-water content from this recorded trace, provided the absolute rainbow intensity is known for a given galvanometer deflection; this absolute value is obtained by comparison with the galvanometer deflection produced by the standard light from mirrors (F) and (G), which is a known fixed fraction of the total light in the collimated beam. Rainbow theory shows that particles illuminated by the beam will send to the photocell a fraction of the total light in the beam which is proportional to the ratio of water content (average mass per unit volume) to drop diameter. As already mentioned in the last section, angular distance from one intensity maximum to the next is directly related to particle diameter. Numerical values for interpreting recorded traces are derived and explained in the appendix.

After experiments with direct photographic recording, an instrument incorporating the essential features of figure 4 was constructed; it was used on a C-46 airplane for icing research conducted by NACA during the latter part of the 1945-46 season. Although the instrument was available for only a few flights at the end of the season, and exhibited some imperfections in details, results were very encouraging. A new model of the instrument, incorporating improvements found desirable as a result of experience with the first instrument, was constructed for use in subsequent flight icing research tests. In the discussions which follow, examples of instrument design details are drawn from this second model of the instrument.

OPTICAL ANALYSIS OF RAINBOW RECORDER

Evaluation of Light Flux Reaching Photocell

Having determined the light intensity due to the fog particles, it is necessary to find what part of this energy is effective in actuating the photoelectric pickup and to analyze the optical requirements of the recorder. A general description of a photoelectric type rainbow recorder has already been given. The geometry of the instrument is detailed in figure 5.

In figure 5, the distance from the center of the scanning mirror to the lens is r_M; also $r' = H/\sin p$ is the distance at any instant from the center of the scanning mirror to the beam axis, along a line making an angle p with the beam axis; and $r = r' + r_M$.

It is now assumed that the photosurface can view the entire vertical height of the beam at all angles of interest. (The term vertical will always refer to the direction perpendicular to the plane of figure 5.) Then any single sphere of water in the field of view and in the beam of light contributes light to the photosurface expressed by

$$(I_p)\ (\pi/4)\ (D^2)$$

where

I_p the light per unit area from a single particle

D the diameter of the viewing lens

The horizontal field of view of the viewing slit is

$$U = u/f_1 \quad \text{radians} \quad (\text{if } u/f_1 \text{ is small})$$

where

u the slit width

f_1 the distance from the slit to the lens

Then the volume of space from which fog particles send light to the viewing slit is

$$(Ur)\ (A/\sin p)$$

where A is the perpendicular cross-sectional area of the light beam at the sample region (fig. 6).

Thus the total light received by the viewing slit from all the particles visible at a single position of the scanning mirror is

$$W_p = (Ur)\ (A/\sin p)\ (n_d)\ (I_p)\ (\pi/4)\ (D^2)$$

where

W_p the total radiation power received by the slit

n_d the number of water drops per unit volume

It is shown in the appendix that

$$I_p/I_B = K_p(d/r)^2$$

or

$$I_p = (K_p)\ (W_B/A)\ (d/r)^2$$

where

W_B the total radiation in the beam (spectrally effective watts)

K_p the intensity factor plotted in figure 2

The number of fog drops per cubic centimeter is

$$n_d = 6(w)\ (10^{-6})\ (\pi\rho d^3)^{-1}$$

where

w the free-water content in grams per cubic meter

d the drop diameter in centimeters

ρ the density of water in grams per cubic centimeter

Substituting values for n_d and I_p into the formula for W_p gives

$$W_p/W_B = (3/2)\ (10^{-6})\ (K_p)\ (U)\ (D^2/rd)\ (w/\rho)\ (\sin p)^{-1}$$

The distance r may be expressed as

$$r \sin p = H\left[1 + (r_M/H)\ (\sin p)\right]$$

where H is the perpendicular distance from the center of the scanning mirror to the beam axis, as shown in figure 5.

Substituting the value of r sin p into the formula for W_p/W_B gives

$$W_p/W_B = \frac{(3/2)\ (10^{-6})\ (K_p)\ (U)\ (D^2/Hd)\ (w/\rho)}{1 + (r_M/H)\ (\sin p)}$$

A typical value at the rainbow maximum is

$$W_p/W_B = (0.69)\ (10^{-7})$$

where

H = 32.6 centimeters

r_M = 7.5 centimeters

p = 39°

D = 3.5 centimeters

U = 0.0175 radians

w = 0.5 grams per cubic meter

d = $20(10^{-4})$ centimeters, 20 microns

K_p = 0.032 (fig. 2)

ρ = 1 gram per cubic centimeter

Note that the distortion of intensity pattern due to change of viewing angle is proportional to the change of the factor $1 + (r_M/H)\ (\sin p)$. In the above mentioned example, as p varies from 30° to 40° the distortion is only about three percent.

In order to deduce free-water content w some particular W_p must be measured on the recorded rainbow curve. This has been taken to correspond to the quantity B_1, defined in figure 3, for which the value of K_p is 0.032. Other variables in the formula for W_p/W_B are readily measurable with the exception of W_B; it is effectively included in the standardizing process.

Effect of Many Particles and of Nonparallel Light

The effect of nonparallel light, of mixed wavelengths, or of mixed drop sizes, is to reduce the relative contrast between maxima and minima of intensity. With visible light, a wavelength distribution range of 40 millimicrons causes a negligible reduction, and hence is effectively monochromatic.

In calculating the effect of mixed particle sizes, a particular type of distribution of water among the various diameters must be

assumed. Experimentally, the distribution in clouds is not far from Gaussian with respect to cross-sectional area as a function of drop size (reference 1). Hence this work considers a distribution expressed by

$$d(w/a)/da = K_o \, e^{[-(2/k)^2 (1-a/a_o)^2]}$$

$$K_o = \frac{d\left(\frac{w}{a}\right)}{da} \text{ at } a=a_o$$

illustrated in figure 7

where

a_o the most frequent (modal) drop radius

dw the water contained in drops having radii between a and a + da

k an arbitrary constant specifying the flatness of the distribution curve

A large value of k corresponds to a large range of drop radii. In terms of the effective limits of drop radii, the parameter k may be expressed as

$$k = (a_2 - a_1)/a_o$$

in which a_2 and a_1 are the two drop radii corresponding to a value of $d(w/a)/da$ which is $1/e$ times the maximum ($e=2.72...$). Hence, k may be considered as the effective relative fractional range of drop sizes. For distributions other than true Gaussian, it is expected that the actual distribution may be sufficiently closely approximated in most cases by an equivalent Gaussian distribution in which the effective range k is determined by the same formula $(a_2-a_1)/a_o$, but where a_2 and a_1 are now defined to be the radii such that the value of $d(w/a)/da$ corresponding to them in the actual distribution is $1/2.72...$ times the maximum.

Interpolating the curves of figure 2 and averaging the intensities using the Gaussian weight factors will lead to a set of "distribution" graphs, of which figure 3 is an example, with $k=0.8$ and $a_o/L=16.1$. They are, of course, calculated on the basis of parallel rays of light. Nonparallel rays whether due to divergence

at the light source or at the point of viewing, cause a further reduction of contrast. This reduction is computed by first averaging one of the series of distribution graphs over the divergence angular range at the source, and then averaging this resultant curve over the divergence at the point of observation. The curves produced after these operations are still essentially similar to the one in figure 3.

In all these curves, the most easily measurable parameter dependent only on average radius is the angle Δp between the first and second intensity maxima. Figure 8 exhibits this relation. For distribution ranges k up to 0.8, the variation of Δp is less than 3 percent for a given particle size.

The quantity most closely associated with the relation between water content and rainbow intensity is the parameter B_1, defined in figure 3. (Parameter B_1 is slightly affected by a normal divergence of 4° as shown in fig. 9.) It is not possible at this point to give the complete relation between water content and rainbow intensity, since the proportionality factor depends also upon instrument characteristics such as spectral efficiency of filters, slit width, lens diameter, etc.; it is derived in the next section. Parameter B_1 is practically unaffected by small drop-size distribution ranges because the angular location of the principal intensity maximum for a single sphere changes very little over the whole range of diameters common in clouds (fig. 2). For large distribution ranges (enough to reduce greatly the contrast ratio B_2/B_1), the calculated water content should be multiplied by a factor of from 1.0 to 1.1 in order to compensate for the reduced amplitude of the primary maximum intensity.

The contrast ratio corresponding to these curves is defined as B_2/B_1

where

B_2 the height of the second rainbow maximum minus the first minimum

B_1 the height of the first maximum minus the height at viewing angle 48°

These quantities are illustrated in figure 3 for the special case of zero divergence. For nonparallel rays corresponding to any one total divergence δ the contrast ratio B_2/B_1 changes principally with the distribution range k as shown in figure 10. The effects of a double-peaked drop-size distribution have not been extensively computed. The general result is a reduction of contrast

considerably greater than that produced by a normal distribution with the same effective limits, although the shape of the intensity curve is not greatly different.

Calculation of Divergence

It can be seen from figure 10 that a large divergence δ leads to such small contrast ratios that evaluation of drop size becomes difficult because of uncertain location of the second maximum. It is therefore important to insure a small value of δ.

The divergence used in figures 9 and 10 is

$$\delta = \delta_s + \delta_v$$

where

δ_s the source divergence

δ_v the viewing divergence

A minimum value

$$\delta s = u_s/h_s \text{ radians}$$

occurs for a perfect lens when the source is at the principal focus (focused on infinity). Similarly,

$$\delta_v = u/h \text{ radians}$$

when the viewing slit is focused on infinity. Here u and u_s denote horizontal width of the viewing slit and of the light source filament, respectively; h_s and h are the focal lengths of the collimating lens and viewing lens, respectively.

In case the viewing slit is focused on the rainbow particles instead of on infinity, the viewing divergence becomes approximately

$$\delta_v = u/f_1 + D/r \text{ radians}$$

It should be noted that the intensity formula for W_p/W_B has

the same form whether the viewing slit is focused on infinity or on the rainbow particles, even though the derivation assumed for convenience that the slit was focused on the rainbow. It is only necessary to observe that

$$U = u/h$$

for focusing on infinity, or

$$U = u/f_1$$

for focusing on the rainbow. In either case, U is the horizontal field of view. Marked advantage of either method of focusing has not been established experimentally.

Failure to have either the source or the viewing slit focused exactly will increase the minimum δ by about 0.3° for each percent shift in distance from the lens, for the case of an f/2 lens. Lens aberration at either source or viewing point can increase δ more than other causes combined. For example, an f/1.5 simple plano-convex lens was found to have spherical aberration equivalent to an effective divergence of about 7° – relatively enormous, as can be seen from the rainbow curves of figure 10. An f/2 projection lens was found to be of satisfactory quality.

A total divergence δ of about 4° is acceptable.

DETAIL DESIGN AND ELECTRICAL ANALYSIS

Arrangement of Instrument Components

Most dimensions of a rainbow instrument are fixed within fairly narrow limits once a particular source of light is assumed. Consider a source collimating lens having a focal length of 3 inches; and assume an AH-6 lamp, with an effective width of about 0.08 inch; then the source divergence becomes 0.08/3 radians, or 1.54°. Hence the 3-inch focal length is satisfactory. Both source and viewing lenses should have as large a diameter as possible without too much aberration. An f/2 lens of 3-inch focal length has been assumed for both source and viewing lenses.

The photosurface height determines the vertical angular viewing range of the observing system. This must be sufficient to cover the

entire height of the collimated light beam at all angles of interest. Consequently, the vertical height of the AH-6 lamp must be stopped down; this has the further advantage of cutting off the flickering electrode regions of the lamp.

The viewing slit width u must be small enough to limit the diverging light behind it to less than the width of the photosurface; this will automatically result in a reasonably small viewing divergence. A value of 0.06 inch has been chosen for u.

The filters have been placed just in front of the slit, between the slit and the viewing lens.

The scanning mirror should not be close enough to the viewing lens to cut off part of the field of view, but a large distance will increase the distortion, due to the size of the factor r_M/H.

An angle of 70° has been chosen for the position of the beam axis relative to the instrument axis (figs. 4 and 5), since this permits a range of viewing angles p from 20° to 50° with a rainbow particle distance from the instrument roughly comparable to the length of the instrument; accordingly, the scanning mirror cam is adjusted to tilt the mirror back and forth between an angle of 45° and an angle of 60° with the instrument axis.

Light Source

The type AH-6 or BH-6 lamp was chosen for the light source because it is capable of furnishing a large amount of light in a narrow band of wavelengths and is sufficiently concentrated to secure a small divergence when used to produce a collimated beam.

Power is supplied to the lamp from an Eclipse 400-cycle 1.5-kva inverter driven from the 28-volt d-c. aircraft power system. When operating, the lamp draws about 1 ampere at 1000 volts or a total of 1 kilowatt. A Peerless special No. 5316 transformer is used to increase the 110-volt output of the inverter to 1200 volts at no load and 1000 volts with a load of 1 ampere.

The mercury lamp is cooled by air discharged from two 0.1-inch orifices. Air is obtained from an electrically driven positive displacement pump and filtered with a painter's type air filter. This assembly delivers 7 cubic feet of oil-free air at 15 pounds per square inch to the lamp.

The AH-6 lamp must be horizontal and have equal amounts of mercury at the two electrodes before starting. A hinged back on the

lamp case makes this possible. When voltage is first applied, the lamp must remain horizontal for a few seconds until it reaches full brilliance. Then the lamp may be safely tilted into its normal position by closing the hinged back of the housing.

A combination of Corning 5551 and 3389 filters placed in series effectively passes the 440-millimicron wavelength band and eliminates all radiations of other wavelengths from both mercury lamp and sunlight. Figure 11 exhibits the separate spectral characteristics of sunlight, mercury lamp, photosurface and filters.

To protect the filters and photocell from direct sunlight striking the mirror, a removable sunshade is included.

Figure 12 is a plot of the joint spectral efficiency of the AH-6 lamp, filters and photosurface and of sunlight, filters and photosurface. The area under either curve is a spectral efficiency factor, with dimensions of millimicrons (i.e., millimicrons times efficiency, efficiency being a dimensionless number).

The effective power in the beam may now be computed from

$$W_B = (F_s)\ (K_e)\ (R_s)\ (K_I)\ (K_t)\ (W_{400})$$

in which

W_B the power in the beam (spectrally effective watts)

F_s the spectral efficiency factor associated with the mercury lamp (fig. 12)

K_e the ratio of the spectral energy radiated by the lamp at 800 cycles per second to the total power supplied to the lamp

where

R_s the ratio of watts per millimicron of wavelength range radiated by the lamp to the total spectral energy in the lamp spectrum

K_I the fraction of light intercepted by the lens

K_t the transmission efficiency for light entering lenses, windows and mirror

W_{400} the total electric power supplied at 400 cycles per second

Numerical values are:

F_s = 6.1 millimicrons (See fig. 12.)

$R_s = 3.75\ (10^{-3})$ per millimicron at 440 millimicrons

K_t = 0.5

K_e = 0.5

K_I = 0.016 for f/2 lens assumed

W_{400} = 1000 watts

Substituting these values in the formula we find

$$W_B = 0.092 \text{ effective watts}$$

Electronics

The electronic circuit consists of four essential units: (1) the photocell, (2) the amplifier, (3) the power supply, and (4) the recording unit.

Apart from the obvious requirements such as linearity, shielding, shock stability, and ease of operation, the special requirements for recording photocell current from a rainbow include: (1) sensitivity sufficient to record a rainbow resulting from light falling on a cloud having a water content of 0.25 gram per cubic meter, with 10 micron drops, and (2) discrimination such that a background light of 2000 candles per square foot will not affect the recorded signal.

Photocell.- It was found that a photomultiplier-type photocell such as the RCA 931-A would solve the problems of sensitivity and shock stability encountered in detecting small amounts of radiation from an artificial rainbow.

It must be noted that there is a definite maximum permissible electron multiplier gain in order that the output current of the phototube due to background light does not exceed the rating of the tube. The 931-A has a rated current of 1 milliampere and a cathode sensitivity of 9 milliamperes per spectrally effective watt. Hence the output current is

$$i_o = 0.009NW = 0.001_{max}$$

and

$$\text{maximum } N = \frac{0.001}{0.009\ W_{max}}$$

where

W the spectrally effective watts of radiation

N the electron multiplier gain

i_o the photocell current in amperes

Radiation reaching the photosurface from the background is computed approximately from

$$W_b = (U)\ (V)\ (D/2)^2\ (B_b)\ (F)\ (K_b)$$

Here

U the horizontal field of view in radians

V the vertical field of view

D the diameter of the viewing lens in centimeters

K_b the transmission efficiency for light encountering two windows, the scanning mirror, and the viewing lens

F a spectral efficiency factor, based on the spectral characteristics of the filters, the photosurface, and sunlight

B_b the background brightness in watts per square centimeter, per millimicron-wavelength range near the energy maximum of sunlight

W_b the spectrally effective radiation (watts) reaching the photosurface.

Assuming dimensions and filters corresponding to the present model of rainbow recorder, as in the previous sample calculation,

U = 0.0175 radian

V = 0.25 radian

K_b = 0.64

$D/2$ = 1.75 centimeters

F = 10.7 millimicrons (fig. 12)

B_b = $1.2(10^{-4})$ watts per square centimeter per millimicron, for 2000 candles per square foot

Substituting these values gives

$$W_b = 1.05(10^{-5}) \text{ spectrally effective watts}$$

The signal due to the spectral energy from the rainbow is negligible compared with the background light in determining the magnitude of the photomultiplier output current. Therefore:

$$N_{max} = \frac{0.001}{0.009W_b} = 10,500$$

The gain of the photomultiplier tube can be adjusted by proper selection of the dynode voltages.

For certain assumed instrument values and cloud density it was shown in a previous section that the spectral energy received from the rainbow is

$$W_p = 0.69(10^{-7}) \ (W_B) \text{ spectrally effective watts}$$

Since the sensitivity of the photosurface is 9 milliamperes per spectrally effective watt, the above formula leads to

$$i_s = 6.2(10^{-10}) \ (W_B) \text{ rms amp}$$

in which i_s is the root-mean-square signal current at the photosurface corresponding to the rainbow maximum. With $W_B = 0.092$ for the sample instrument

$$i_s = 5.7(10^{-11}) \text{ rms amp}$$

at the photosurface. The signal current from the photomultiplier due to modulated light from the rainbow is then

$$Ni_s = 10,500 \ i_s = 0.59 \text{ rms microamp}$$

This current is therefore the approximate maximum input to the amplifier.

Two very serious difficulties were encountered in the use of the photomultiplier which will be encountered to a greater or lesser extent with any emissive-type photocell. These difficulties are: (1) fatigue and (2) interference of background light through shot effect.

The cesium surface photomultipliers were found to have a very rapid rate of fatigue or loss of gain with use. The rate of

fatigue is a function of current drawn by the last dynode and time of exposure. The current drawn is in turn a function of voltage applied to the tube, and total light reaching the photosurface. If left in the dark for a period of 1.5 to 3 times the length of the exposure, the tube will completely recover.

The effects of fatigue may be compensated by following the photomultiplier with a variable gain amplifier which may be adjusted either automatically or manually to keep the over-all gain of the system constant. This compensation is effective until the photo-tube has deteriorated to the point that saturation occurs. Then the instrument should be rested or the tube replaced. Fortunately, this instrument is designed so that during one-half of each cycle (while the standard pulse is being applied), the background light is eliminated. This reduces the rate of fatigue many times.

The operator must be careful never to allow light to fall on the photocell continuously, while the instrument is not in use. A cover is provided for the photocell aperture to exclude sunlight while the instrument is inoperative.

The second difficulty encountered in the use of the 931-A was the high value of the shot effect current resulting from intense background energy levels (1500 to 2000 cp/sq ft).

The shot effect (an alternating component of current due to random statistical fluctuations of the electron flow within the tube, discussed in reference 2) places a lower limit upon the intensity of the rainbow light which can be interpreted by conventional circuits. The modulated rainbow current must be many times greater than the root mean square value of shot effect current, if the record is to be free of interference. The shot effect is considered quantitatively in the discussion of the amplifier.

Amplifier.- It is evident that a narrow band pass would be advisable in the amplifier. The minimum band width that can be used is determined by the shape of the modulated envelope of the 800-cycle rainbow signal current, the rate of sweep, the permissible distortion of recorded rainbow curve, and the frequency stability of the 400-cycle source of current for the mercury arc lamp.

A Fourier analysis of the rainbow intensity curve indicates that distortion of less than 2 percent will be obtained if the fifteenth harmonic of the sweep frequency is passed by the circuit without attenuation.

The sweep frequency in the latest instrument is approximately 2 cycles per second. The required band for this sweep frequency is 140 cycles per second.

Knowing the minimum band width which will be passed by the tuned amplifier and the maximum d-c. background anode current of the photomultiplier tube, the shot effect may be calculated from the following formula which is an empirical generalization of the formula in reference 2:

$$i_r = \left[(E)\ (i_c)\ (f)\ (n!) \right]^{\frac{1}{2}}$$

where

i_c the average cathode current in amperes

f the band width of the tuned amplifier, cycles per second

E the charge on an electron

n the number of electron multiplications

i_r the root mean square value of shot effect current.

Numerical values are

$E = 1.6 \times 10^{-19}$ coulomb

$n = 8$ (determined by the number of dynodes in the phototube)

$f = 140$

$i_c = 0.009\ W_b = 0.95 \times 10^{-7}$ at 2000 candle power per square foot (See section on photocell.)

for which

$$i_r = 3.0 \times 10^{-10}$$

The corresponding phototube cathode signal current was shown in the discussion of the photocell to be of the order of magnitude of $5.7(10^{-11})$ root mean square ampere.

This gives a signal to noise ratio of $\frac{0.57}{3.0} = 0.19$ which is much lower than the required ratio of 50 or greater for an undistorted record.

Since signal to noise ratio was found to be too low for practical use, a system to balance out the noise due to shot effect was developed. According to the formula used to predict shot effect, the magnitude of the shot effect current is independent of frequency but depends only on band width. This fact is made use of in the rainbow amplifier to reduce or eliminate shot effect.

The final amplifier actually consists of two separate amplifier channels both of which are driven from the output of the photocell. One amplifier is tuned to 800 cycles with a band pass sufficient to amplify the rainbow signal undistorted. Besides amplifying the signal, a component of shot effect whose amplitude is a function of the band pass is amplified also.

The second amplifier is tuned to a second frequency at which no appreciable components of the rainbow signal exist. A frequency of 2600 cycles was chosen since there is no harmonic component of the 800 cycles at this frequency and it is far enough removed from the 800-cycle channel that there is no overlap of band pass.

The output of the second amplifier contains only shot effect. The rectified outputs of these two amplifiers are combined in such a manner as to give a reading of the difference of the two signals in the recording mechanism. If the band width times gain of the two amplifiers are equal, the root-mean-square value of shot effect in the 2600-cycle channel will be equal to that of the 800-cycle channel. Therefore, the two will cancel, leaving only the rainbow signal which is the difference between the two signals.

The circuit of the amplifier is shown in figure 13. The input terminal is connected directly to the anode of the photomultiplier. The 0-1 d-c. milliammeter in the input lead indicates total background light falling on the photocell by measuring the d-c. current drawn by the last dynode. A 6SF5 high mu triode is used as an untuned input stage. The potentiometer in the grid of the 6SF5 is used as a master gain control for the unit. This tube is followed by two 6V6's connected as triodes with the grids of the two tubes paralleled and the plates connected to an 800-cycle filter and a 2600-cycle filter, respectively. The outputs of these filters are detected by the balanced bridge plate detector circuit which rectifies and takes the difference between the 800-cycle and the 2600-cycle signals.

Thorough precautions were found necessary to make certain that no harmonic distortion occurred in any of the early stages of amplification. It was found that harmonic distortion in any of these stages would produce components of the 800-cycle signal which would be amplified by the 2600-cycle channel and cause a negative

deflection of the meter, resulting in a nonlinear output.

Except for this, the circuit is all quite straightforward. It might be noted that in paralleling the triode sections of the 6N7's in the plate detector circuit, one triode section of one tube was paralleled with one triode section of the other in order that uneven weakening of the tubes would not affect the balance of the detectors. Potentiometers in the grid circuits of the 6N7's are used to adjust the gains of the two channels to offset any inequalities in the two channels so that the shot effect will be accurately canceled in the output. It is necessary, occasionally, to make small adjustments in these settings as the tubes age or some other circuit constant changes.

As has been previously mentioned, in order to eliminate the interference due to shot effect, it is necessary to have band width times gain of the 800-cycle channel equal to that of the 2600-cycle channel. The band width of the channel is fixed by design but the gain may be varied by use of the gain controls in the 6N7 grids in order to compensate for small differences in band widths or changes of circuit constants affecting gain. To balance the amplifier, a source of unmodulated light is focused on the photocell so that 1 milliampere of d-c. current is drawn by the anode. The 6N7 gain controls are then adjusted until the output meter gives zero deflection, indicating that shot effect is balanced out. The total gain is then adjusted by use of the master gain control until the maximum rainbow signal or the standardizing signal, whichever is larger, gives full-scale deflection of the galvanometer.

The film drive switch is closed when the viewing screen indicates conditions are proper for recording. Due to its low impedance and consequent freedom from electro-magnetic pickup, the galvanometer may be remotely located along with the film drive switch.

Periodic observation of the shape and height of the standard pulse will check performance of the entire instrument, especially the mercury lamp. Undue random variations, or markedly reduced amplitude for a given attenuator setting, may indicate lamp deterioration. Reduced amplitude of the standard pulse can also result from reduced voltage applied to the electron multiplier, tuned amplifier, or fatigue of the multiplier tube.

The 1500-ohm helipot in the plate circuit of the 6N7's is used to adjust the zero setting of the recording galvanometer. Once adjusted, this setting will probably not need to be changed.

Recording Galvanometer.- The recording galvanometer is an NACA

medium sensitivity type, suitable for use in flight, with a sensitivity of about 300 microamperes for full-scale deflection when unshunted. A suitable shunt is used to produce full-scale deflection on 35-millimeter film when 3 milliamperes are applied. Separate film drums of 200-foot capacity are used, driven by a small 20-volt governor-controlled d-c. motor. A film speed of about 1 or 2 inches per second is preferred if the complete mirror scanning cycle is 1 second. The recording galvanometer case has a visual observation screen which may be used simultaneously with the film recording.

Power Supply.- The power for the photomultiplier and the amplifier is supplied from two genemotors which deliver 600 volts regulated and filtered d-c. to the photomultiplier and 250 volts regulated and filtered d-c. to the amplifier. Filament voltage is obtained by use of a dropping resistor in the 28-volt supply.

Figure 14 shows the instrument installed in a C-46 airplane. The amplifier power supply and the inverter, transformer, and air compressor for the AH-6 lamp are remotely located and do not appear in the picture.

INTERPRETATION OF RECORDS

Recorded traces should look similar to the calculated curve of figure 3, provided the fog density is reasonably uniform during the scanning cycle. Other deviations will usually be due to electromagnetic pickup, microphonics, nonuniform film speed, or unsteady mercury-lamp intensity, caused by voltage fluctuations in the 400-cycle power supply. Also, when a very bright and nonuniform cloud background is being scanned by the viewing mirror, some harmonics of the resulting current pulses will be within the band pass of the 800-cycle tuned circuit and hence will be amplified. This condition may occur on entering or leaving a cloud.

Drop size is obtained by finding the difference in viewing angle between the first two rainbow maxima and referring to the curve of figure 8. In order to do this from the recorded curves, the angular scale must be found as a function of distance along the film. Since the limits of mirror oscillation are known, the length on the film for a scanning cycle can readily be interpreted in terms of mirror angle, and hence of viewing angle.

The ratio of free-water content to drop diameter is directly proportional to the ratio of rainbow primary maximum height to standard height, with both measured from the rainbow height at viewing angle 48°. The constant of proportionality can be determined from (1) rainbow theory in conjunction with laboratory measurements of the fixed fraction of the collimated beam seen by the

photocell through the standard channel, or (2) calibration of the whole instrument against simultaneous measurements of fog-particle diameter and free-water content by an independent means. Method 2 is described in the next section. When compared with method 1, it provides an over-all check on rainbow theory, as well as a calibration for the individual instrument being tested.

Standardization

In the standardization of the power ratio of W_p/W_B it is desirable to eliminate the effects of (1) changes in frequency or intensity of the light source, and (2) change in amplification of photomultiplier or tuned amplifier. This is done by periodically shining a fixed fraction of the collimated beam of light through the filters and on to the photocell (fig. 4). This fraction should be comparable to the light from an average rainbow.

A spring-loaded cam-operated shutter, synchronized with the scanning mirror, cuts off the rainbow and inserts the standardizing signal during the reverse half of each cycle. Determination of the value of this fixed fraction of the beam may be done in the laboratory by a straightforward geometric method external to the instrument itself; for example, by attenuating the beam through two small holes, and simultaneously directing it into the instrument by means of a mirror.

In applying the results of this laboratory standardization, correction will have to be made for reflection losses at any windows added for use in flight or other field operation. Fog condensation, dirt, or oil on these windows must be avoided. It may be necessary to eliminate the windows if it is impracticable to heat them to eliminate fogging.

EXPERIMENTAL RESULTS

The early model photoelectric rainbow recorder was used for preliminary calibration measurements. For checking the accuracy of rainbow theory, simultaneous measurements of drop diameter and free-water content were made by the rainbow recorder and an alternative method. This was done at night in a fog on Mt. Hamilton, California, in January 1946. Flash microphotographs were used to observe fog-particle diameter and distribution. Free-water measurements were obtained by drawing a known volume of air through steel wool mesh and immediately weighing the increased mass. The efficiency of the filter was checked by drawing the same sample of air through two filters, consecutively. The increase in mass was

entirely in the first filter, indicating that the air entering the second filter was dry.

Errors in such a check are mainly due to time lag in performing the different operations. Microphotographs were taken within 1 to 5 minutes, free-water measurements within 5 to 10 minutes, of the rainbow records during fog conditions that remained nearly constant for 1 hour.

Drop diameters were about 19 microns, and the free-water content was approximately 0.3 grams per cubic meter. Observed range of drop-size distribution was from about 0.8 to 1.2 times the most frequent diameters.

Since w/d is proportional to d^2, average particle diameters measured from the film negatives must be weighted, with respect to area in comparing them with average size deduced from the rainbow traces.

Drop diameters deduced from the rainbow curves differed by 2 percent, on the average, from diameters measured on the micro-photograph negatives. Free water measured by the collection method was 0.31 ± 0.03 gram per cubic meter; corresponding free water indicated by the rainbow maxima was 0.29 ± 0.03 grams per cubic meter. The agreement thus appears to be within the limits of error. However, for the instrument used, the 2-percent diameter agreement is probably fortuitous and 5 percent is more likely.

Drop-size distribution ranges k obtained from the micro-photographs were quite consistent with the shape of the recorded rainbow traces, although high divergence, due to the lenses used at the time (about 7° each), made it impossible to determine k accurately from the rainbows. More extensive experimental checks of this point are desirable.

Comparisons were also made in a fog chamber in which a uniform fog of somewhat controllable characteristics could be obtained. Microphotographs were used to check particle diameter, and free-water measurements were made by allowing the free water to settle upon an absorbant plate of known area. This measurement assumed that the vertical column of water directly above the plate would be collected upon the plate. A correlation of 5 percent was obtained between the two systems for measuring drop diameter. The water-content measurements agreed within 10 percent. Some typical records taken in the fog chamber are shown in figure 15. These records were taken over a period of 3 minutes in a fog which was allowed to settle out of the atmosphere. The larger drops settled first, causing the mean-drop diameter and drop-size distribution range to

become smaller. The last strip in figure 15 shows records taken with a distribution range approaching zero which gives contrast ratio of approximately 1.2 (as shown in fig. 10 for divergence equal to 4°), or a second maximum of which the intensity is 120 percent of the intensity of the first maximum. This series of records shows the agreement which has been obtained between the shape of actual records and the mathmetically predicted curves.

The present model rainbow recorder was installed on a C-46 airplane, and operated for a few flights during the latter part of the 1946-47 icing season.

Comparative measurements of liquid-water content and drop size were obtained by the rotating cylinder technique. Ice collected on four rotating cylinders inserted into the air stream for a known time interval is preserved and weighed. Altitude and airspeed are recorded also. Drop size and free-water content may be deduced from these cylinder data by means of aerodynamic theory, summarized in reference 1, provided the temperature of the cylinders is at least several degrees below freezing. Average diameter measured by the cylinder method is weighted with respect to fog-particle volume. The rainbow method gives an average which is weighted with respect to fog particle area.

Owing to the inherent difference in the basis of averaging, some difference in average drop size by the two methods might be expected with the cylinders tending to give the larger values.

Numerical data on accuracy of agreement between the two methods is presented here for a cylinder run.

	Average drop size	Water content
Rotating cylinders	15 microns ±0.8	0.42 gm/m^3 ±0.02
Rainbow recorder	14 microns ±0.8	0.40 gm/m^3 ±0.04

Rainbow recorder data were averaged from a number of rainbows recorded during the time the cylinders were collecting ice for 1 minute in an exceptionally uniform cloud. Errors in the rotating-cylinder measurements stated above are estimated from the precision with which it is possible to observe the recorded quantities which enter into a calculation of water content or drop size. Theoretical errors or systematic instrumental errors are not included. Limits of error stated for the rainbow method are estimated from experience

with the calibration employing microphotographs and fog collector measurements.

DISCUSSION

In addition to its uses in icing research in flight, the rainbow recorder should find application in the general study of clouds and fogs under conditions in which the instrument remains stationary. For this work the present equipment would probably give adequate results. It has been suggested that it might be used also in the study of particle size and distribution in carburetion problems and chemical problems dealing with liquid aerosols. (For particles other than water, the rainbow theory must be recomputed for an appropriate index of refraction.)

The use of the instrument as a flight instrument in its present form is found to be complicated by the fact that many of the clouds encountered in flight prove to be so nonuniform that the variations in cloud character, even during the short one-half-second scanning period of the recorder, cause "hash" in the rainbow record which usually completely obscures the shape of the rainbow trace. This condition was studied by making traverses through various clouds with the mirror fixed at one angle so that any variations in the galvanometer trace were due to nonuniformities in the cloud structure scanned as the airplane moved through the cloud. The variations in the trace so measured with fixed mirror were frequently found to be greater in amplitude than the variations in the normal rainbow trace would have been for a uniform cloud.

Observations were made to decide whether any optimum rate of scanning could be determined. This is believed to be impossible, since the "cloud hash" seems indiscriminate as to frequency. No sweep rate could be found which would give a range of rainbow modulation frequencies at which there would be no cloud hash. Components of cloud hash have been found having periods of as long as 30 seconds and as short as 1/30 second. Since 30 cycles per second is the highest frequency to which the galvanometer will respond, there is no reason to assume that components of much higher frequency do not exist. With the present scanning rate of 2 cycles per second, satisfactory rainbow traces should result during all periods when the cloud, as seen by the instrument, is uniform for a period of a second or more. However, it is difficult to be certain which cycles of the trace are usable and which are distorted by cloud hash.

Several systems have been conceived to apply the rainbow recorder to nonuniform clouds with greater certainty.

Experiments are being initiated on a comparatively simple addition

to the present instrument which will record light from the same segment of cloud as the rainbow recorder observes, but at a constant viewing angle. This record will be traced simultaneously with the rainbow record by means of a second galvanometer element on the same film. From the fixed angle record it can be determined whether the cloud was uniform during the period of any sweep, thereby allowing the operator a means of deciding the validity of an apparently good record. If no record appears to be valid, then the operator may plot a third curve of the ratio between the two recorded curves. This will give the true shape of the rainbow curve if drop diameter is constant during the period of measurement and only water content is varying. If this procedure proves successful, an electronic device can be developed which will automatically record this ratio.

Another possibility has been suggested, that is, to move the apparent point of observation in the opposite direction of the airplane motion by use of more than one rotating mirror in order to allow a complete record to be taken of one segment of fog. The mechanical arrangement would undoubtedly be difficult to build and operate.

In summary of the results and discussions of this investigation it may be concluded that the fundamental soundness of the rainbow recorder theory has been proved by reasonably good agreement with several comparisons and checks against independent methods of measuring free-water content and drop diameter of fog. It is hoped that further development of the instrument will remove the limitations to its use in flight.

Ames Aeronautical Laboratory,
National Advisory Committee for Aeronautics,
Moffett Field, Calif.

APPENDIX

MATHEMATICAL ANALYSIS OF THE RAINBOW

Intensity Pattern of Light Scattered by a Single Sphere of Water

The rainbow can best be analyzed by first determining the light-intensity distribution produced by a single water drop which scatters plane monochromatic light waves. It was found that the qualitative rainbow theory of Airy, presented at some length by Humphreys (reference 3), proves inadequate in the range of drop sizes from 10 to 50 microns of most common occurrence in clouds. While the details of Airy's theory are of interest only to specialists, its prominence as

the one elementary mathematical description of rainbows easily found in the literature seems to justify a brief explanation of its rejection. The principal simplifying assumption of Airy's theory is that the light intensity is constant over a sufficiently large region of the reflected wave surface of figure 1. To the contrary, it can be shown that the intensity at the wave surface varies extremely rapidly near the cusp, and is nowhere perfectly constant. (See fig. 16.) Airy's theory also assumes that the shape of the wave surface cross section sufficiently near the cusp can be approximated by a cubic curve. This can be true only for particles much larger than those in clouds. Finally, the coordinates used in Airy's theory refer to an infinitely long circular cylinder of water, rather than to a sphere, and therefore the theory can give only a qualitative indication of intensity.

Calculation of the intensity of light scattered by a single transparent sphere employing the electromagnetic theory with accurate spherical boundary conditions (reference 4) is easily carried out only for droplets smaller than about one-half micron. Length of the series needed for 5-micron drops has prevented evaluation in a reasonable period of time. However, a program was started to check and supplement the pioneer work of B. Ray (reference 5) on 2-micron drops. Disagreement was found with Ray's numerical results; the great length of this method was more thoroughly realized; and computations using the electromagnetic theory with rigorous spherical boundary conditions were abandoned.

It was then decided to attempt an approximate analysis assuming that Snell's sine law of refraction holds at the spherical boundary of the particle, although this law is a strict deduction from the electromagnetic theory only for a plane boundary of infinite extent, with perfect dielectric media of infinite depth on both sides. This procedure has proved satisfactory, since it happens that the plane boundary assumption is not greatly in error for drops larger than about 10 microns.

When the shape and intensity of the reflected wave surface near the sphere have both been computed using Snell's law, the distant light intensity is found from diffraction theory by integrating over the wave surface.

Shape of the wave surface near the drop.- In reference 3 there is presented a derivation of the shape of the first completely emergent constant-phase surface, which results when a plane wave of monochromatic light is twice refracted and once internally reflected by a transparent sphere; it is assumed that Snell's sine law of refraction holds at the tangent plane where a light ray intersects the spherical surface boundary, and also that the plane mirror law of reflection holds at the tangent plane where a light ray

is internally reflected. The cusped line of figure 1, if revolved 360°, is such a constant-phase surface computed for an index of refraction 4/3. The index of refraction of water is 4/3 for a wavelength of 0.58 microns, and is within about one-half percent of this for all visible light. The whole constant-phase surface will be denoted by the symbol σ, while the line itself will be termed γ. Using rectangular coordinates x,y positive in the third quadrant, the line γ is determined by the following parametric expressions:

$$x/a = \cos(4q - g) + G \cos(4q - 2g)$$

$$y/a = \sin(4q - g) + G \sin(4q - 2g)$$

where

$\sin g = m \sin q$

$G = 4m(1 - \cos q) - (1 - \cos g)$

m index of refraction

g angle of incidence

q angle of refraction

a radius of the sphere

Intensity of the wave surface.- The ratio of the intensity at the wave surface σ to the intensity in the incident beam may be calculated from the ratio of infinitesimal areas between limiting rays of the incident and emergent flux. Of course reflection or transmission loss must also be considered at the three places on the spherical surface where the rays change direction. A standard formula of the electromagnetic theory (e.g., Handbook of Chemistry and Physics) which refers to an infinite plane interface and unpolarized light states that

$$R = \frac{1}{2}\left[\frac{\sin^2(g - q)}{\sin^2(g + q)} + \frac{\tan^2(g - q)}{\tan^2(g + q)}\right]$$

in which is the fraction of the incident energy reflected at the interface. The resultant fraction of incident light transmitted

through two refracting boundaries and reflected internally at the back boundary of the sphere is

$$R(1 - R)^2$$

The element of area corresponding to the incident flux is

$$2\pi \ (a \sin g) \ d \ (a \sin g) = 2\pi \ a(a/2) \ (\sin 2g) \ dg$$

The element of area corresponding to the emergent flux is

$$2\pi \ y \ ds$$

where ds is an element of length along the line γ, given by the formula $ds^2 = dx^2 + dy^2$. The ratio of these two elements of area is

$$\frac{(\sin 2g) \ dg/d(s/a)}{2(y/a)}$$

Thus

$$I_s/I_B = \frac{R(1 - R)^2 \sin 2g}{2(y/a) \ d(s/a)/dg}$$

where

I_s intensity at the wave surface σ, at a distance s from the x-axis, measured along the line γ

I_B intensity of the incident beam of light

In figure 16, the quantity $2(y/a)(I_s/I_B)$ is plotted as a function of s/a,

where

a radius of the sphere

s distance along the line γ, measured from the x-axis

The intensity plotted in figure 16 is arbitrarily terminated at a point near the cusp, although the mathematical expression goes to infinity. When this intensity is used for finding the amount of radiation at a point distant from the sphere, the intensity is integrated at a constant value for points near the cusp; this value is chosen so that the issuing energy is the same as that under the infinite curve between the same limits along the wave front. The limits chosen must be close together compared to a wavelength.

Surface integral determination of intensity at a distant point.- When the surface σ is observed at a large distance, the intensity as a function of angle of viewing is not obtained merely by extending a line normal to σ and noting the corresponding intensity at σ as given in figure 16. Instead it is necessary to take account of the interference between light waves originating at different parts of σ. This intensity at a distant point is found by means of a mathematical refinement of the Fresnel-Huygens Principle, which states that any surface of constant phase may be considered as sending out spherical wavelets from every part of the surface, whose vibrations reinforce or cancel one another at the point of observation depending on their phase relations. The electromagnetic theory of radiation provides a perfectly rigorous diffraction formula - at any rate, for systems larger than atomic size - analogous to the Fresnel-Huygens Principle (reference 6):

$$V_P = (1/4\pi) \iint \left[r^{-1} (\exp -2\pi j r/L) \underline{\nabla P} - P \underline{\nabla (r^{-1} \exp -2\pi j r/L)} \right] \underline{n} \, dM$$

where

dM an element of area

$\underline{n}$ a unit vector normal to dM

r distance from dM to the fixed point of observation

j imaginary unit $(-1)^{\frac{1}{2}}$

L wavelength

P any component of the electromagnetic vector, evaluated at dM, and may be identified with the vibration displacement in the simple wave theory of light

V_P vibration displacement at the point of observation

∇ the gradient

The integral is taken over any closed surface surrounding the fixed point of observation. There are no restrictions except that P must be continuous and differentiable at every point of the surface of integration.

To apply this general diffraction formula to the case in which light is reflected from a droplet of water, the element dM is taken to be an element of area of the surface σ. (See fig. 17.) The displacement P is evaluated at σ, and may be written

$$P = (I_s)^{\frac{1}{2}} e^{[(2\pi j/L)\ (ct-z)]}$$

where

I_s light intensity in the vicinity of dM

c velocity of light

t time

z distance measured normal to σ, and is positive in the direction of travel of the light wave

Note that the absolute value of the complex number P is $(I_s)^{\frac{1}{2}}$; then the absolute value of V_P is $(I_p)^{\frac{1}{2}}$, where I_p is the light intensity at the point of observation. Substituting the above expression for P into the diffraction formula and performing the indicated vector differentiations in the integrand gives the following approximate expression for Vp, in which the integration is restricted now to the surface σ, since P is zero over the remainder of the closed surface surrounding the point of observation:

$$V_P = (j/2)\iint_\sigma \left\{[\,1+L/(2\pi j z_1)\,] + [\,1+L/(2\pi j r)\,]\cos(n,r)\right\}$$

$$\left\{(1/rL)\ (I_s)^{\frac{1}{2}}\ e^{[(2\pi j/L)\ (ct-z-r)]}\right\}\ dM$$

where

z_1 distance from any element dM to the x-axis, along the normal to dM

(n,r) angle between the direction of r and the normal to dM

The distance z_1 is approximately equal to the droplet diameter d.

Several approximations may be made in the integrand. First, since the point of observation is distant from the droplet, and L is about 0.5 micron, $2\pi r$ is much greater than L. Second, since the droplet diameter is assumed greater than 10 microns, $2\pi z_1$ is greater than L. Finally, the integrand contributes little to the whole integral except when dM is near a point of stationary phase, where $\cos(n,r) = 1$. It has been shown by calculation that only small error is caused by assuming $\cos(n,r) = 1$, provided the droplet diameter is greater than about 10 microns. These approximations lead to a much simpler expression for V_P:

$$V_P = j \iint_\sigma (1/rL)\ (I_s)^{\frac{1}{2}}\ e^{[(2\pi j/L)\ (ct-z-r)]}\ dM$$

In this integral, L is constant; r has small percent change during integration; and the exponential time factor is independent of the variables of integration. The distance z+r in the exponential factor determines the phase of the vibration due to dM that is observed at the distant point. Since dM has been taken to be an element of σ, which is a surface of constant phase, z is constant during the integration. Finally, z+r may be replaced by Z, where Z is the distance from dM to any fixed plane, Z=0, which is normal to the r-axis. This is permissible because only the relative phase is needed. The use of Z instead of z+r is equivalent only to changing the zero from which t is measured. Intensity is independent of phase, since it depends only on the absolute value of the complex number representing the vibration displacement. Substituting Z for z+r, and factoring constant coefficients out of the integrand gives

$$V_P = j(1/rL)\ \ e^{(2\pi jct/L)} \iint_\sigma \ (I_s)^{\frac{1}{2}}\ e^{(-2\pi jZ/L)}\ dM$$

The vibration displacement V_P is a complex number whose phase is of no significance for finding intensity. Its amplitude or absolute value is obtained by taking the product of the absolute values of the complex number factors on the right-hand side of the above formula. The absolute value of a complex number is the square root of the sum of the squares of the real and imaginary parts. As already noted

$$|V_P| = (I_p)^{\frac{1}{2}}$$

then

$$(I_p)^{\frac{1}{2}} = (1/rL)\left| \iint_\sigma (I_s)^{\frac{1}{2}} \cos(2\pi Z/L)\ dM - j \iint_\sigma (I_s)^{\frac{1}{2}} \sin(2\pi Z/L)\ \ dM \right|$$

Therefore, taking the indicated absolute value, squaring, and dividing by the beam intensity I_B:

$$I_p/I_B = \left[(1/rL) \iint_\sigma (I_s/I_B)^{\frac{1}{2}} \sin(2\pi Z/L)\ dM \right]^2 + \left[(1/rL) \iint_\sigma (I_s/I_B)^{\frac{1}{2}} \cos(2\pi Z/L)\ dM \right]^2$$

The quantities in brackets are the fundamental expressions for calculating interference patterns, and will be denoted by S and C, respectively.

Thus

$$I_p/I_B = S^2 + C^2$$

It is convenient for later derivations to have S and C in terms of ratios with respect to the drop radius a.

Then

$$S = (a^2/rL) \iint_\sigma (I_s/I_B)^{\frac{1}{2}} \sin\ [(2\pi a/L)\ (Z/a)]\ dM/a^2$$

$$C = (a^2/rL) \iint_\sigma (I_s/I_B)^{\frac{1}{2}} \cos\ [(2\pi a/L)\ (Z/a)]\ dM/a^2$$

To evaluate the above surface integrals by two successive single integrations, it is necessary to express dM/a^2 and Z/a as functions of the two coordinates which fix position on σ; namely, s and T, where s is distance from the x-axis along the line γ, and T is the "longitude" angle denoting rotation about the x-axis. In the rest of the integrands, a and L are constant, and $(I_s/I_B)^{\frac{1}{2}}$ has already been expressed as a function of s. Since $(I_s/I_B)^{\frac{1}{2}}$ is symmetrical about the x-axis, for unpolarized light, it is of course independent of the angle T. The plane T=0 has been taken to coincide with the xr plane. On the line γ, the coordinates x,y are not independent, for both are functions of s. The r-axis is fixed during integration, but the xy plane is taken to be at an angle T with the xr plane.

Now the x-axis, the point of observation, and the position of the droplet are all fixed during integration. Since the point of observation is distant, the r-axis does not change direction

appreciably for various positions of dM on σ, and therefore the r-axis may be considered to make some constant angle, p, with the x-axis during integration (fig. 17).

To evaluate Z, some definite point along the r-axis must be assumed for the arbitrary reference plane, Z=0, from which Z is measured. This point has been chosen so that the plane Z=0 contains the point of intersection of the x-axis with the front boundary of the droplet (fig. 17), since this leads to the simplest expression of Z in terms of x and y. The plane Z=0 has already been mentioned as being normal to the r-axis; thus its intersection with the xr-plane makes an angle $(90^\circ - p)$ with the x-axis. The distance Z from the plane Z=0 to the element dM of σ may be found by a three-dimensional geometric analysis using the above definitions:

$$Z/a = \left(\frac{x}{a} - 1\right) (\cos p) + (y/a) (\sin p) (\cos T)$$

where (x,y,T) are the coordinates of dM, variable during integration. A simple geometric consideration also shows that

$$dM/a^2 = (y/a) (dT)\, d(s/a)$$

Substituting these values into the expressions for S and C, integrating with respect to T from 0 to 2π, and noting that

$$\int_0^{2\pi} \sin(Y \cos T)\, dT = 0$$

$$S = (2\pi a^2/rL) \int_\gamma (y/a) (I_s/I_B)^{\frac{1}{2}} \sin(X)\, J_0(Y)\, d(s/a)$$

$$C = (2\pi a^2/rL) \int_\gamma (y/a) (I_s/I_B)^{\frac{1}{2}} \cos(X)\, J_0(Y)\, d(s/a)$$

where

$$X = 2\pi (a/L) (x/a - 1) (\cos p)$$

$$Y = 2\pi (a/L) (y/a) (\sin p)$$

$$J_0(Y) = (1/2\pi) \int_0^{2\pi} \cos(Y \cos T)\, dT$$

Here $J_0(Y)$ is the Bessel function of zero order. The integrals are taken along the line γ.

The Bessel function $J_0(Y)$ can be approximated well by the first term of its asymptotic expansion if Y is greater than 10; this will be the case for droplet sizes and angles of interest, provided integration is not carried out for values of y/a less than 0.25. This restriction does not affect the accuracy appreciably, since negligible contribution to the integral come from regions so near the x-axis. The Bessel function then becomes

$$J_0(Y) = (L/y)^{\frac{1}{2}} (1/\pi) (\sin p)^{-\frac{1}{2}} \cos(Y - \pi/4)$$

Substituting this value of $J_0(Y)$ into the expressions for S and C, and defining a new coefficient in the integrand:

$$S = (a/r) (2a/L)^{\frac{1}{2}} (\sin p)^{-\frac{1}{2}} \int_\gamma Q \sin(X) \cos(Y - \pi/4) \, d(s/a)$$

$$C = (a/r) (2a/L)^{\frac{1}{2}} (\sin p)^{-\frac{1}{2}} \int_\gamma Q \cos(X) \cos(Y - \pi/4) \, d(s/a)$$

where

$$Q^2 = 2(y/a) (I_S/I_B)$$

(Q^2 plotted in fig. 16)

Expanding $\cos(Y - \pi/4)$ and transforming products of trigonometric functions into sums

$$S = (a/2r) (a/L)^{\frac{1}{2}} (\sin p)^{-\frac{1}{2}} \int_\gamma Q [\sin(X + Y) + \sin(X - Y) - \cos(X + Y) + \cos(X - Y)] \, d(s/a)$$

$$C = (a/2r) (a/L)^{\frac{1}{2}} (\sin p)^{-\frac{1}{2}} \int_\gamma Q [\sin(X + Y) - \sin(X - Y) + \cos(X + Y) + \cos(X - Y)] \, d(s/a)$$

It has been shown that since the $X - Y$ terms give rise to no stationary phase as s is varied, their contributions may be omitted with quite negligible error. Substitution of the $X + Y$ values of S and C into the formula $I_p/I_B = S^2 + C^2$ gives an expression that may be considerably simplified by cancellation of plus and minus terms after expanding the squares

$$I_p/I_B = (a/r)^2 \ (a/L) \ (2 \sin p)^{-1} \left\{ \left[\int_\gamma Q \sin(X + Y) \, d(s/a) \right]^2 + \left[\int_\gamma Q \cos(X + Y) \, d(s/a) \right]^2 \right\}$$

Defining a new coefficient, the above formula may be expressed as

$$I_p/I_B = K_p (d/r)^2$$

where

$$d = 2a$$

and

$$K_p = (a/L) \ (8 \sin p)^{-1} \left\{ \left[\int_\gamma Q \sin(X + Y) \, d(s/a) \right]^2 + \left[\int_\gamma Q \cos(X + Y) \, d(s/a) \right]^2 \right\}$$

The intensity corresponding to K_p as previously expressed is that due to the first internal reflection of light entering a sphere of water. Other light reflected in the general direction of the rainbow comes from the front surface of the drop. These front surface light rays are nowhere strongly concentrated, and as a result they merely add a little to the general illumination without giving rise to any notable interference effect. The increased brightness is too small to measure accurately.

The integrals in the expression for K_p have been evaluated by plotting the integrands in terms of s/a and planimetering the areas. Sufficiently few oscillations of the integrand occurred so that accuracy was retained. Numerical values of K_p have been computed as a function of p, for three typical drop sizes, and appear in figure 2.

REFERENCES

1. Tribus, Myron and Tessman, J. R.: Report on the Development and Application of Heated Wings, Addendum I. AAF Tech. Rep. 4972, Add. I, Jan. 1946.

2. Terman, Frederick Emmons: Radio Engineers' Handbook. First Edition. McGraw-Hill Book Co., 1943, p. 292.

3. Humphreys, W. J.: Physics of the Air. Third Edition. McGraw-Hill Book Co., 1940, Chapter III, pp. 476-500.

4. Lord Rayleigh: The Incidence of Light upon a Transparent Sphere of Dimensions Comparable with the Wavelength. Proceedings of the Royal Society, Series A. vol. 84, Apr. 1910, pp. 25-46.

5. Ray, Bidhubhusan: The Scattering of Light by Liquid Droplets, and the Theory of Coronas, Glories, and Iridescent Clouds. Proceedings of the Indian Association for the Cultivation of Science, vol. 8-9, 1923-26, pp. 23-46.

6. Smythe, William R.: Static and Dynamic Electricity. First Edition. McGraw-Hill Book Co., 1939, Chapter 13, Problem 10.

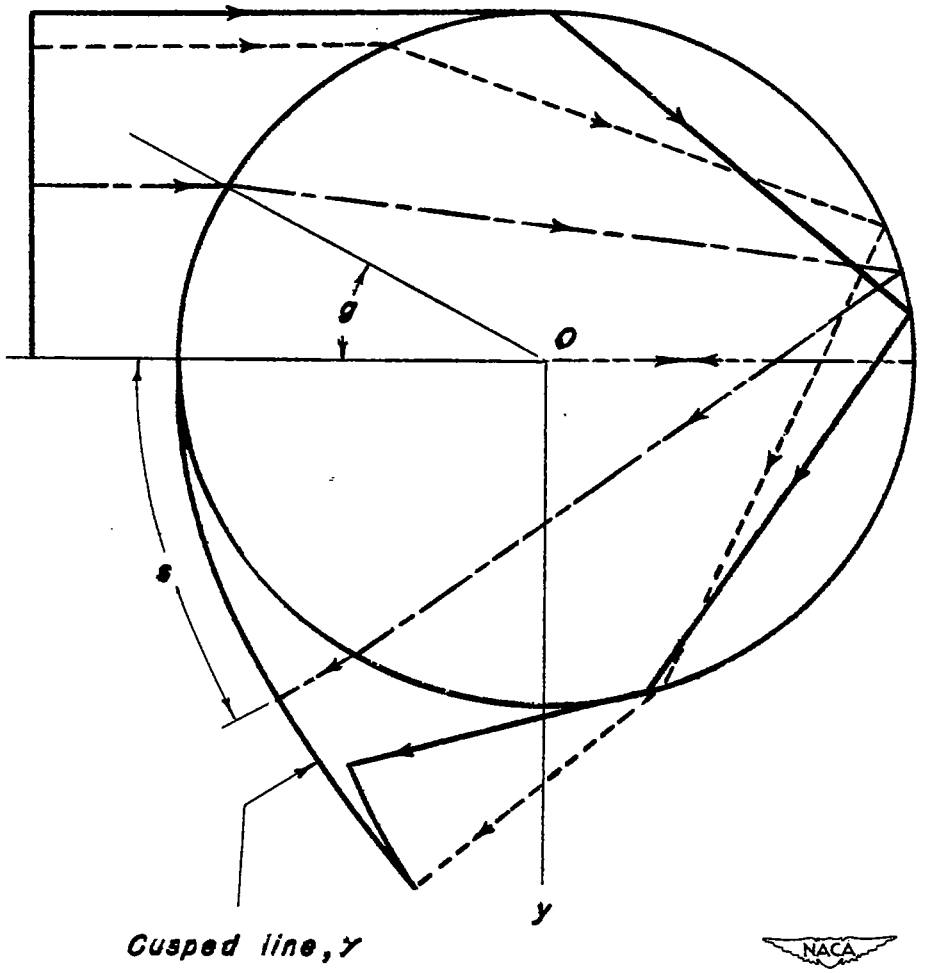

Figure 1.- Ray paths, and wave shape of emitted wave near surface of a transparent sphere.

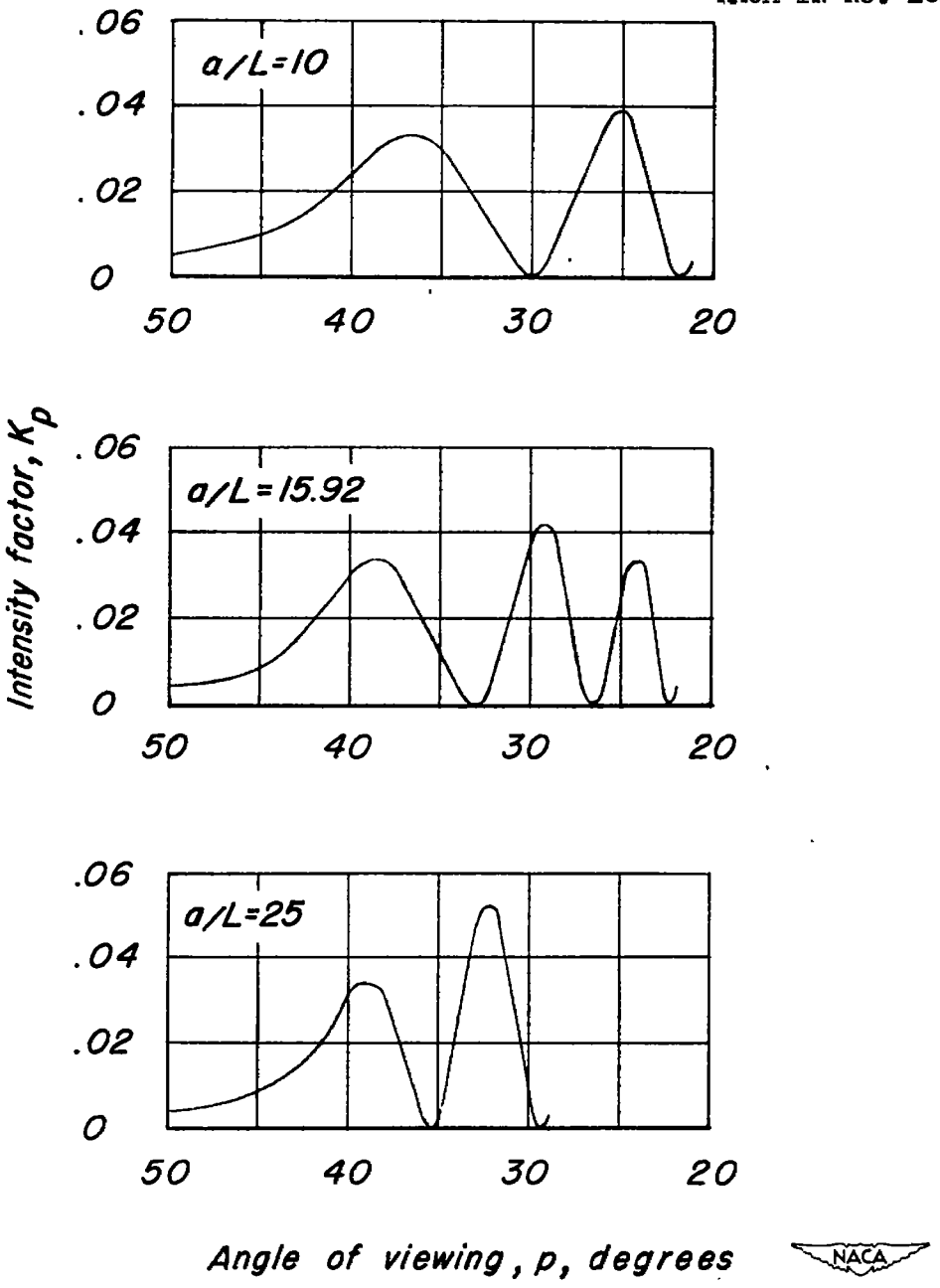

Figure 2.- Variation of light intensity with angle of viewing for a single drop and parallel light, for different ratios of drop radius to wave length, (a/L).

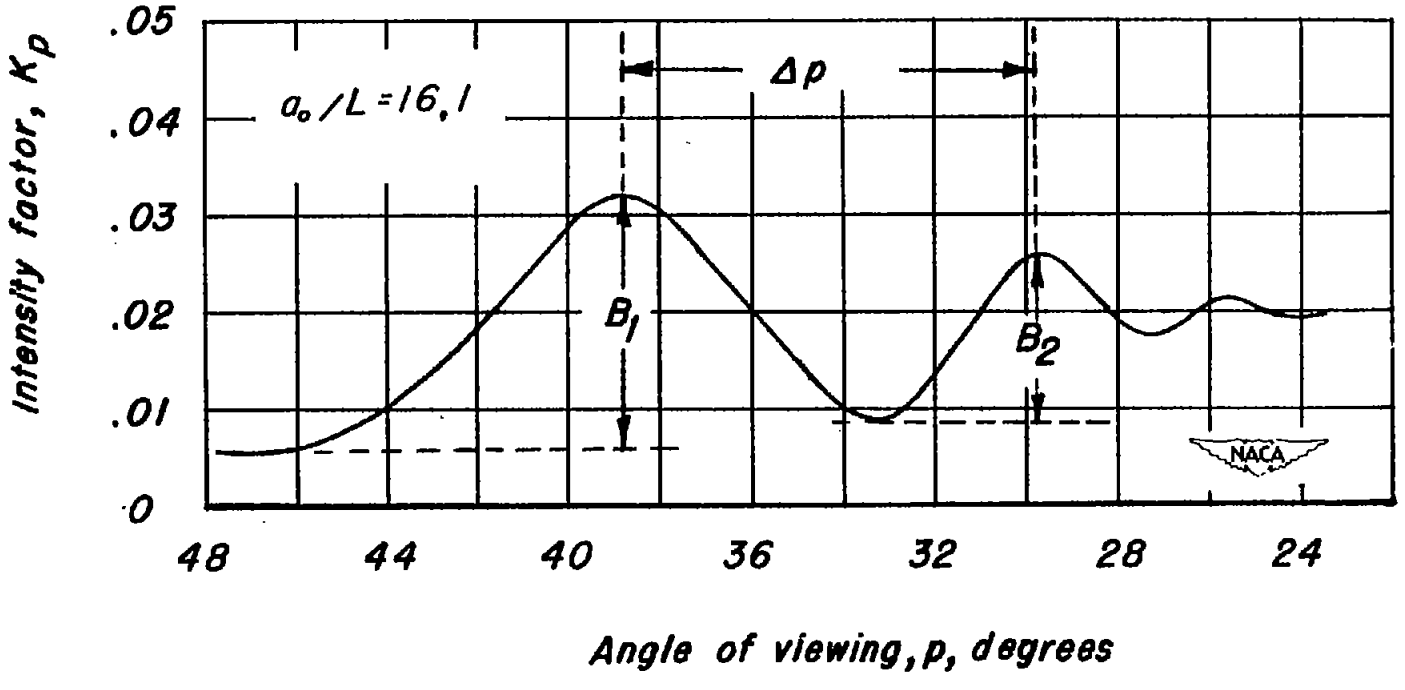

Figure 3.- Calculated light intensity distribution for mixed drop sizes assuming parallel light for k = 0.8.

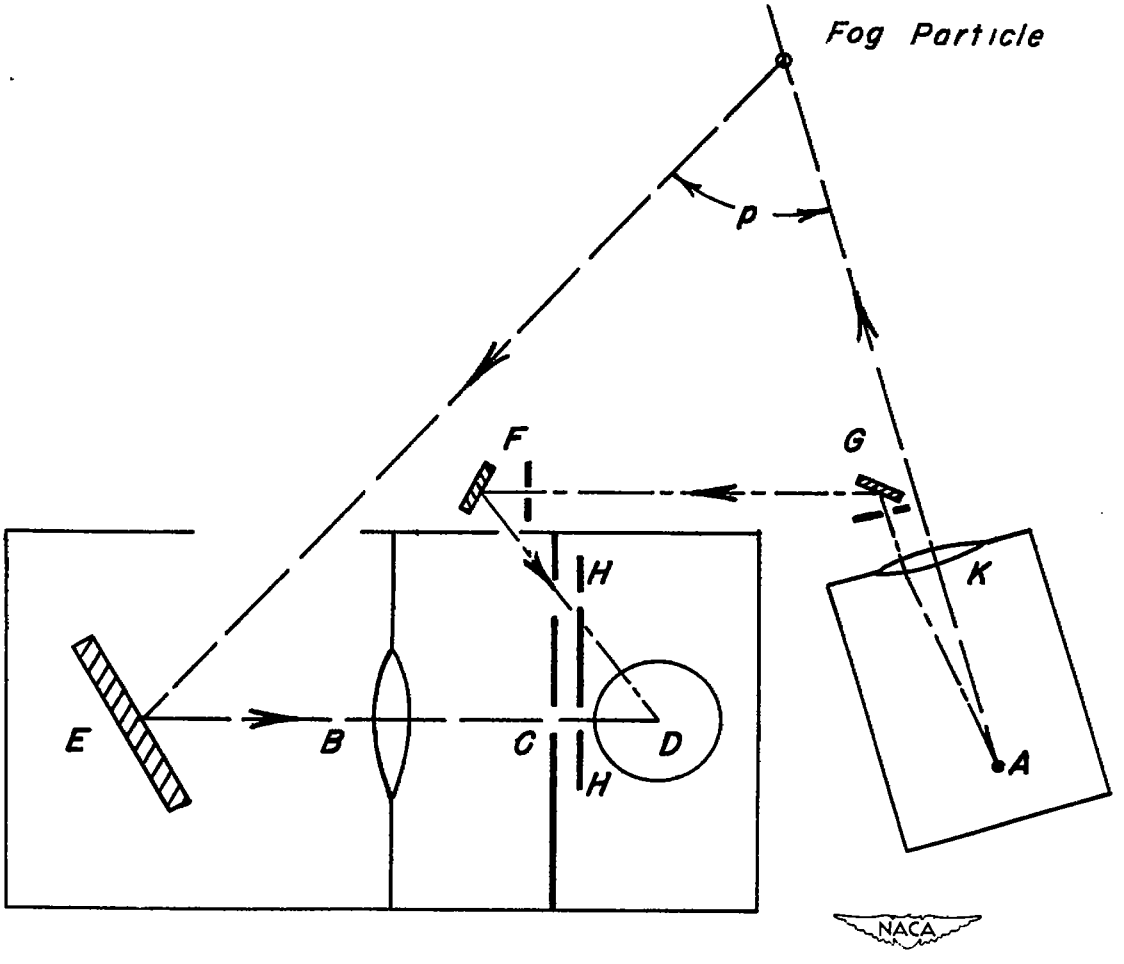

Figure 4.- Schematic diagram of optical arrangement of photoelectric rainbow recorder.

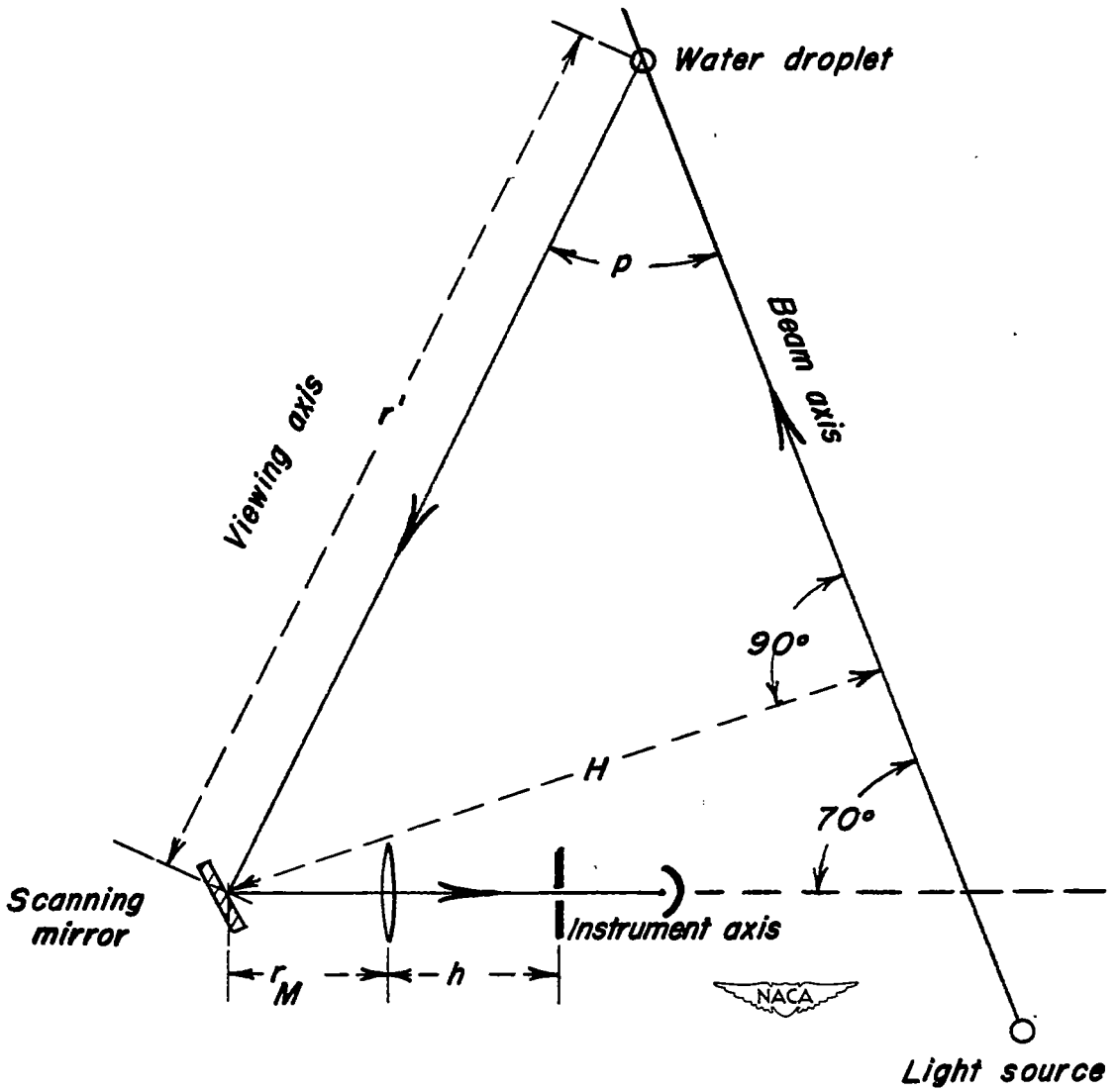

Figure 5.- Schematic diagram of rainbow recorder for describing distances and angles used in geometric analysis of light intensity at photocell.

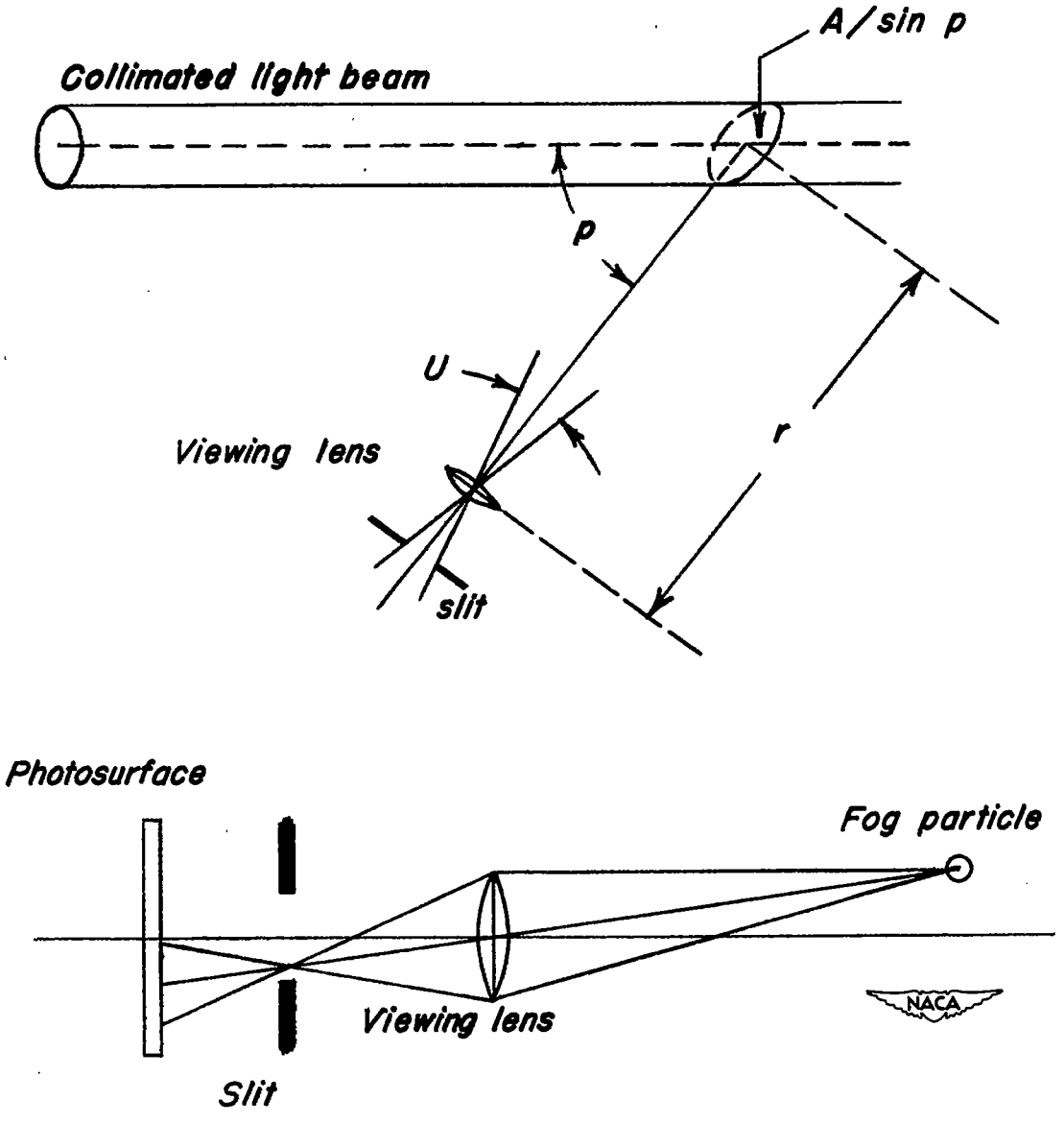

Figure 6.- Schematic diagram illustrating angles and distances useful in calculating light reaching the photocell.

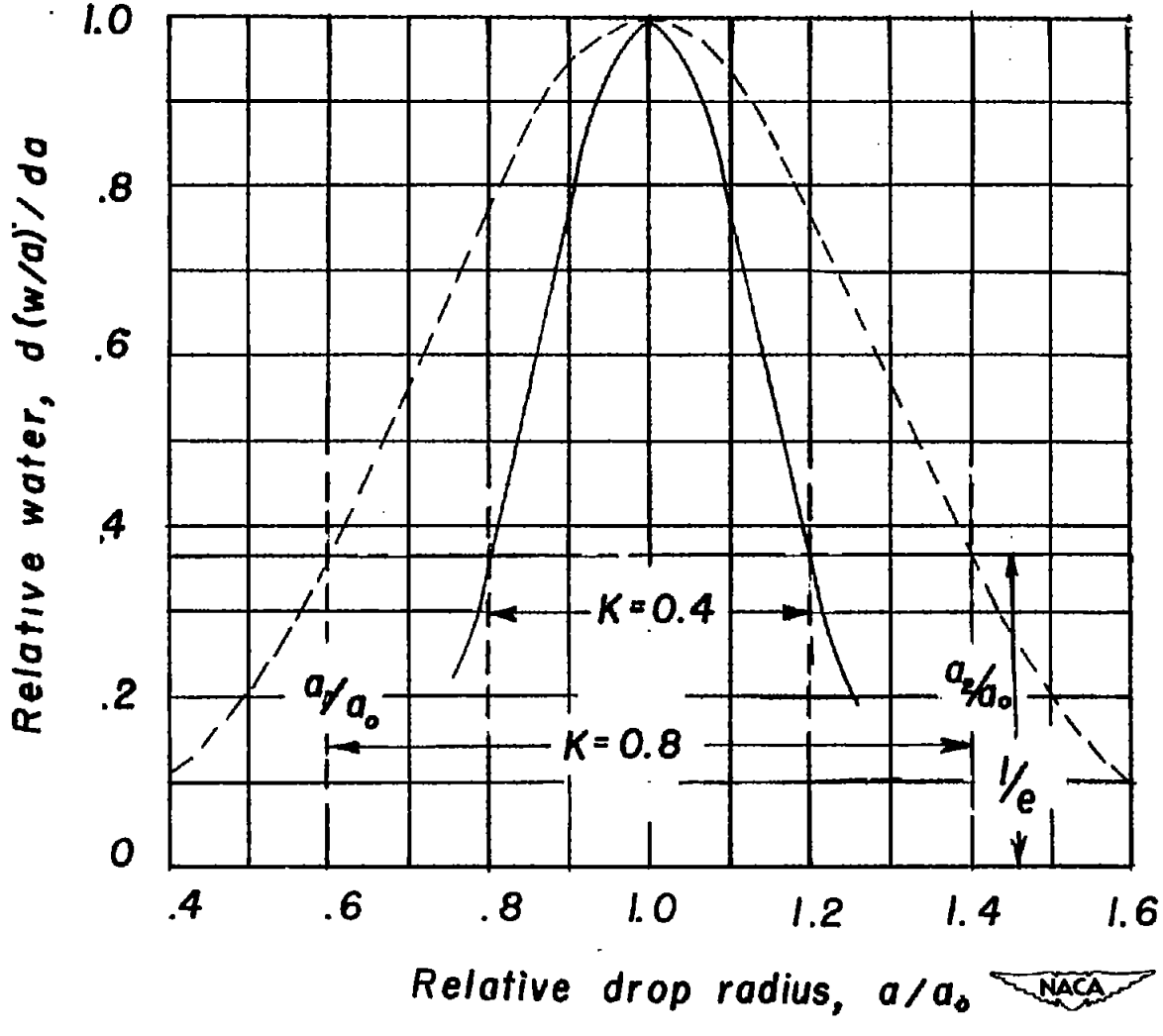

Figure 7.- Graph of Gaussian distribution function.

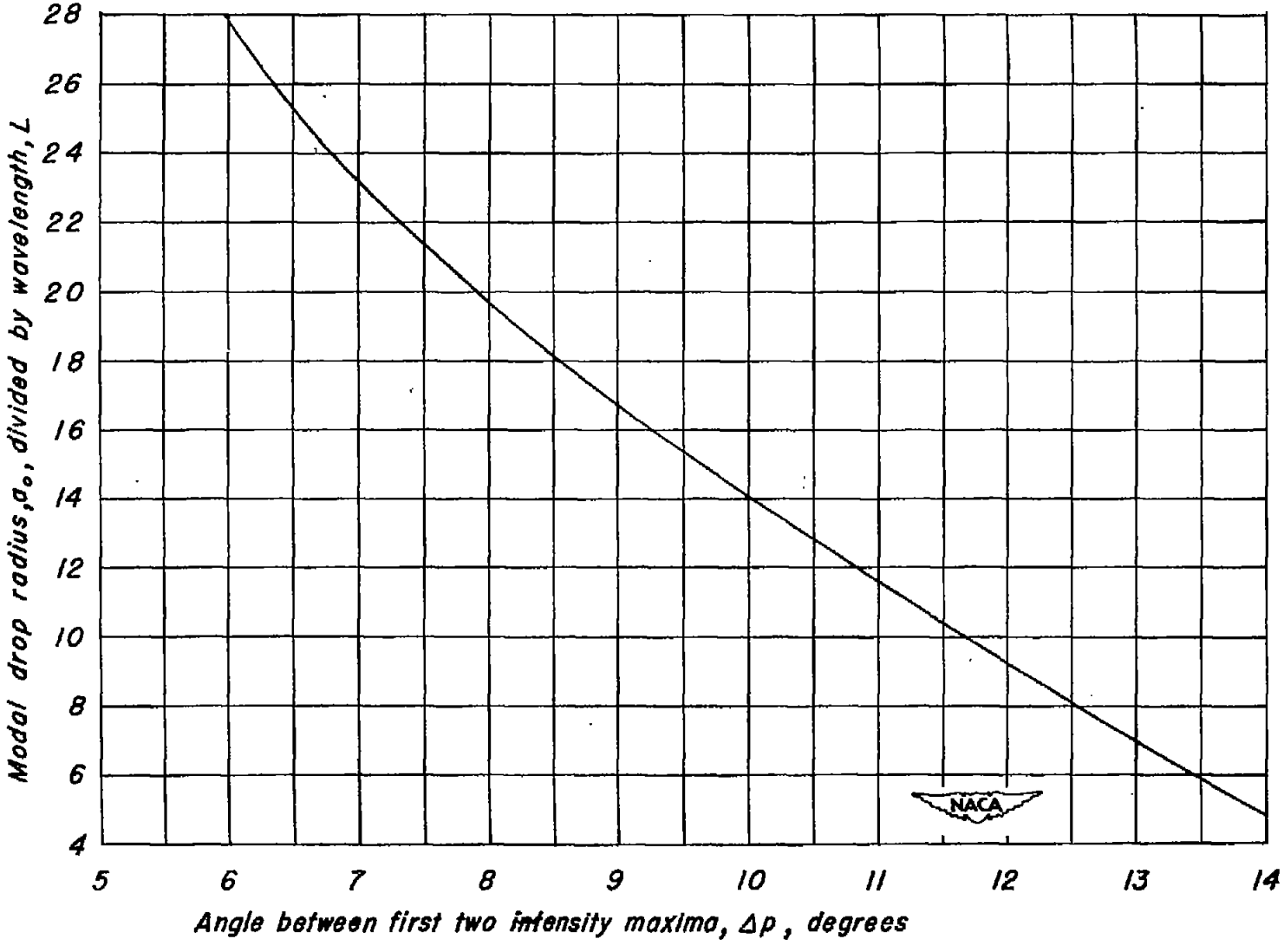

Figure 8.- Relation between drop size and band spacing.

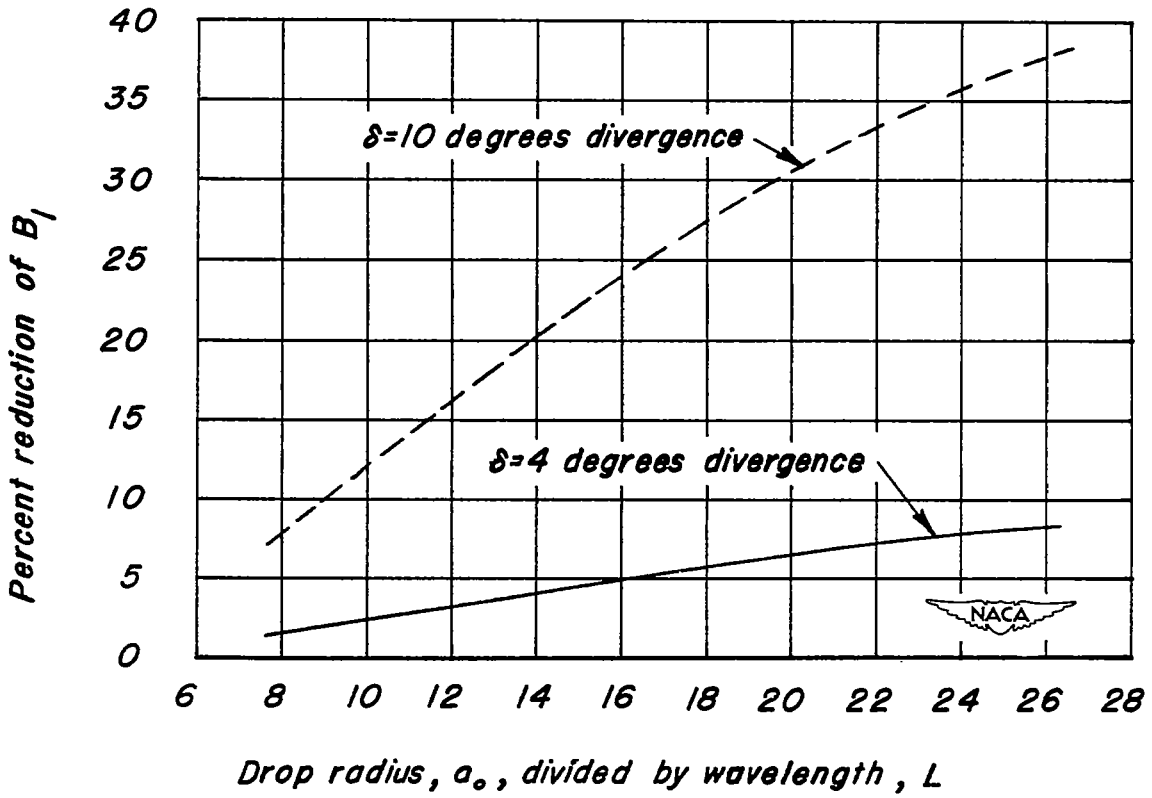

Figure 9.- Change of maximum intensity due to divergence; initial value of B_1 is 0.030; δ is the source divergence plus viewing divergence.

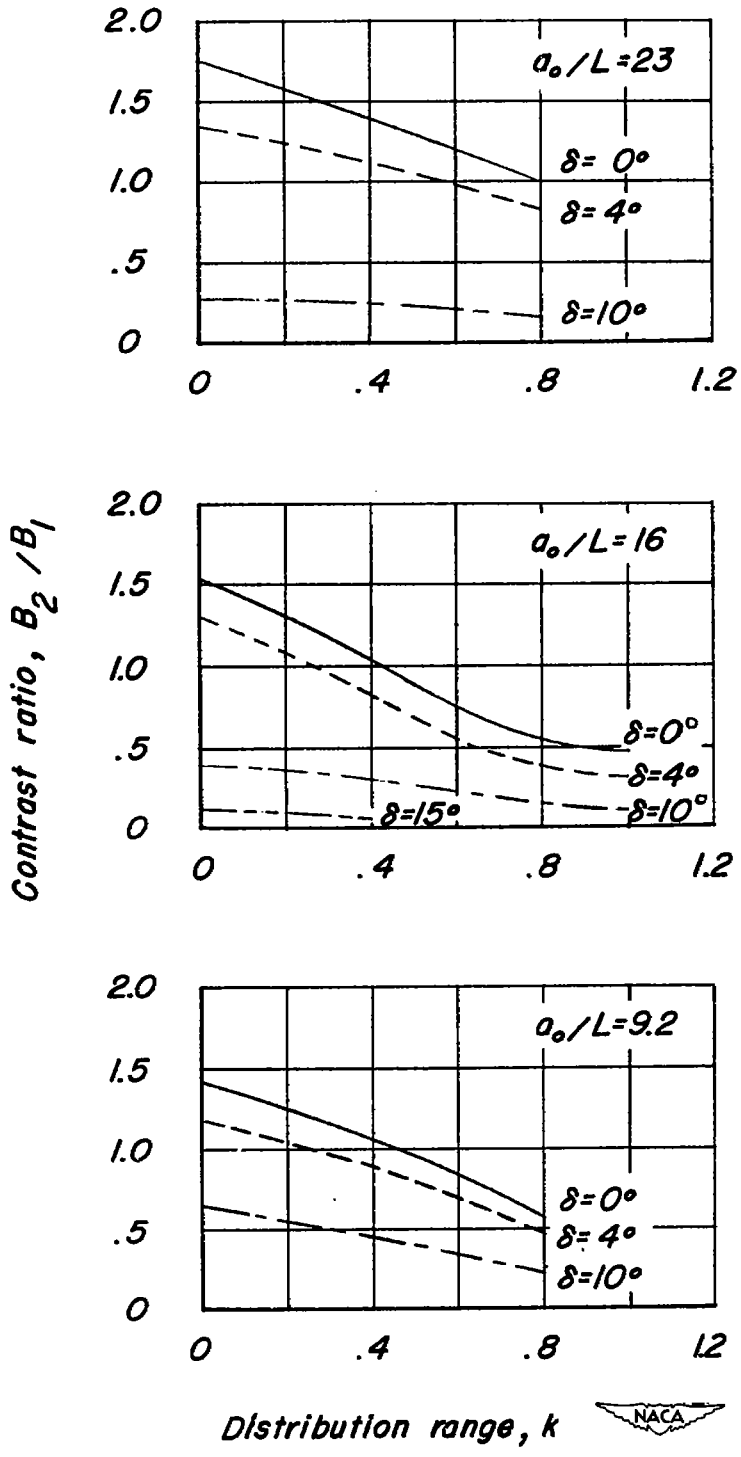

Figure 10.- Relation of contrast to drop-size distribution range.

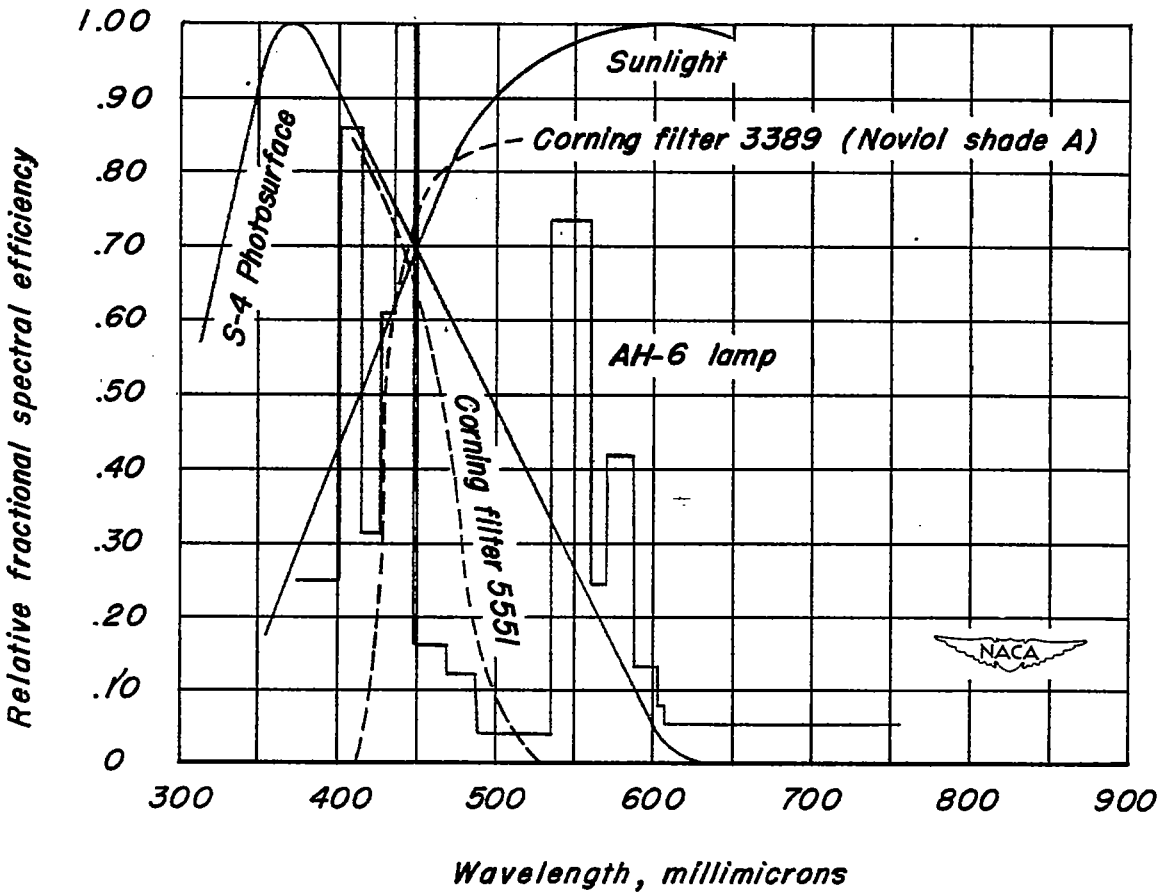

Figure 11.- Spectral efficiency as a function of Wavelength: AH-6 lamp from G.E. instructions pamphlet; S-4 photosurface from RCA tube handbook; Corning filters from Corning catalogue.

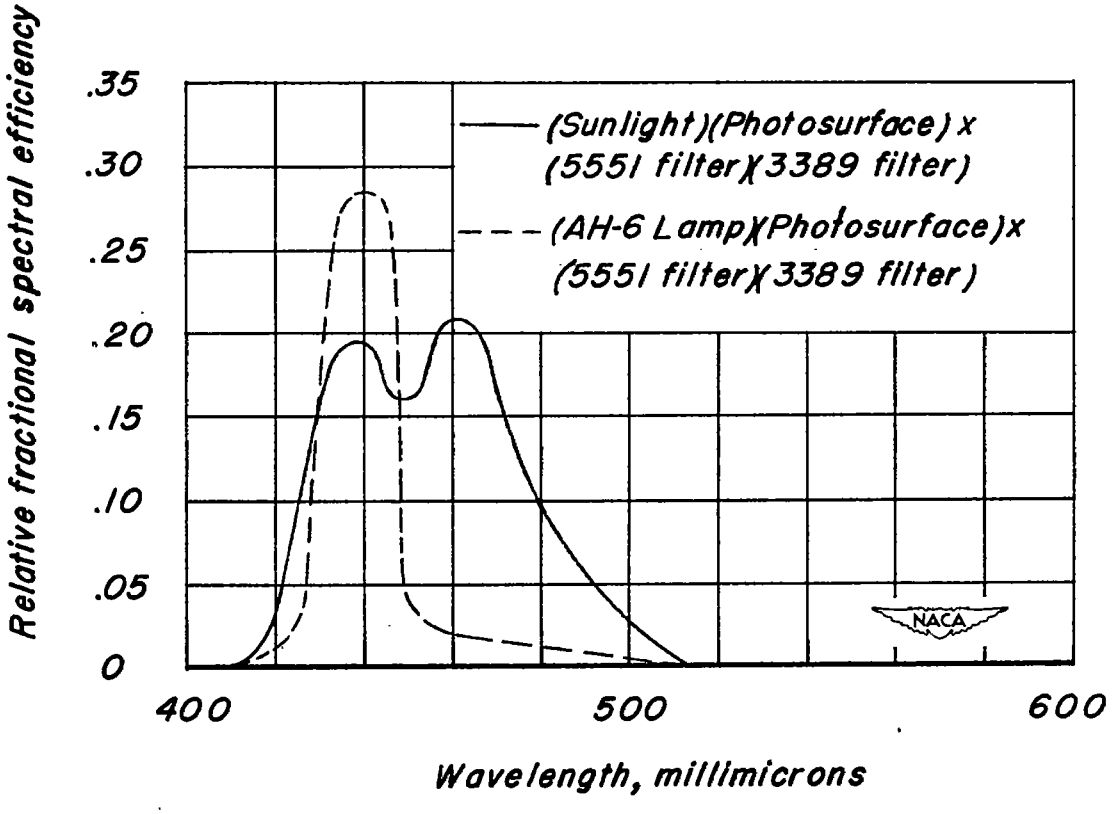

Figure 12.- Joint spectral efficiency as a function of wavelength.

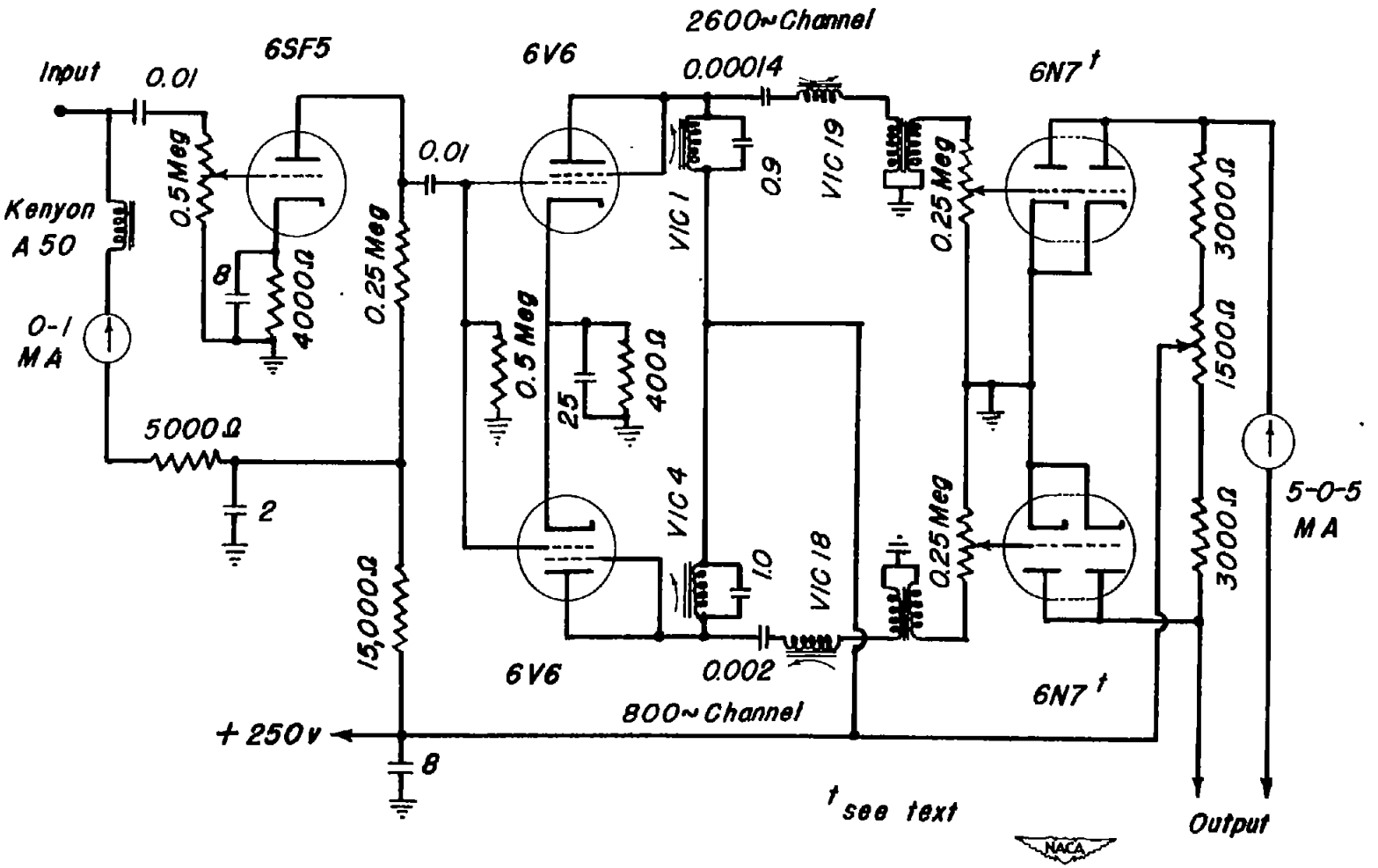

Figure 13.- Circuit diagram of 800 cycle amplifier with shot effect eliminating channel.

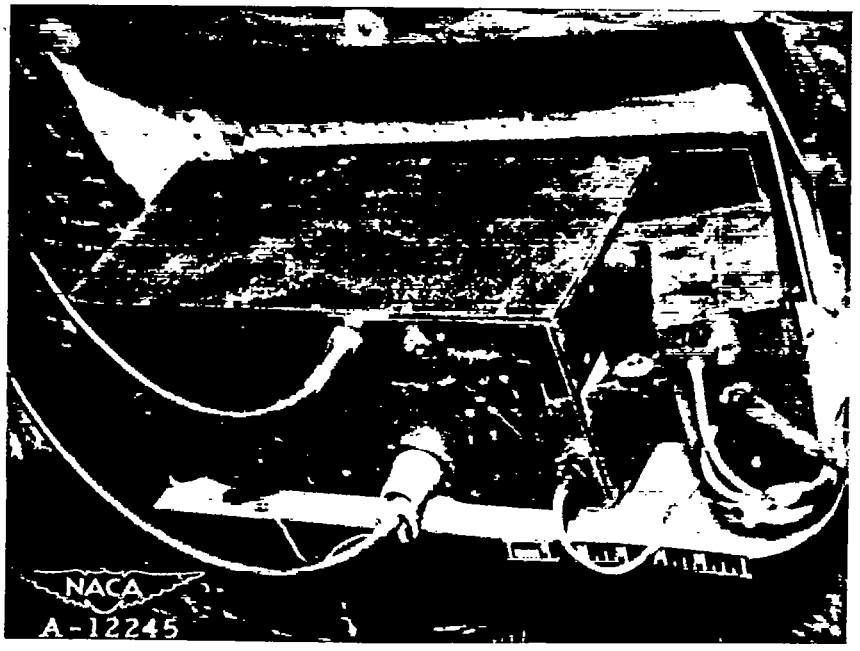

(a) Light source, mirror and photocell.

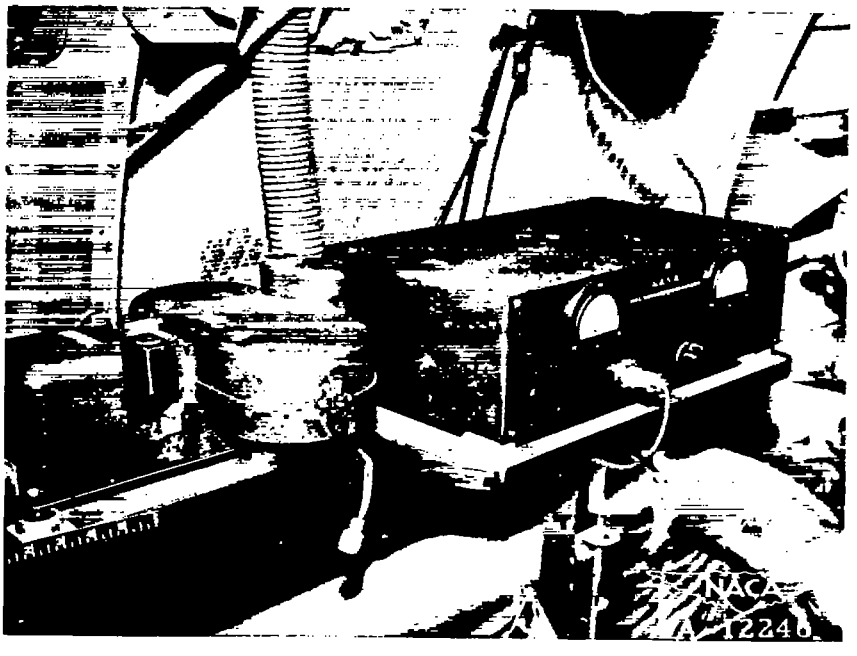

(b) Amplifier and recording galvanometer.

Figure 14.— Rainbow recorder installed in C—46 airplane.

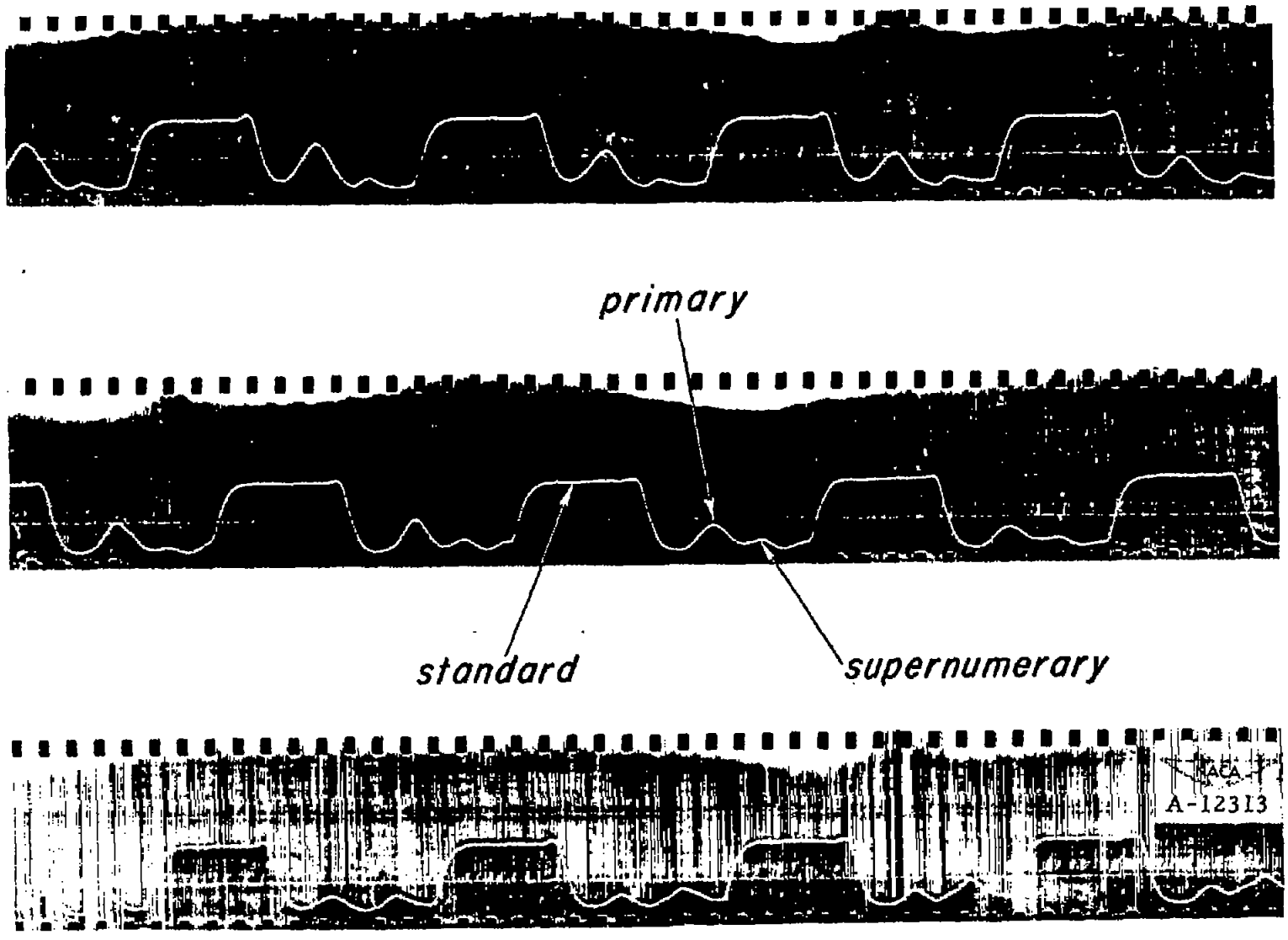

Figure 15.— Typical rainbow records taken in fog chamber over 3 minute period.

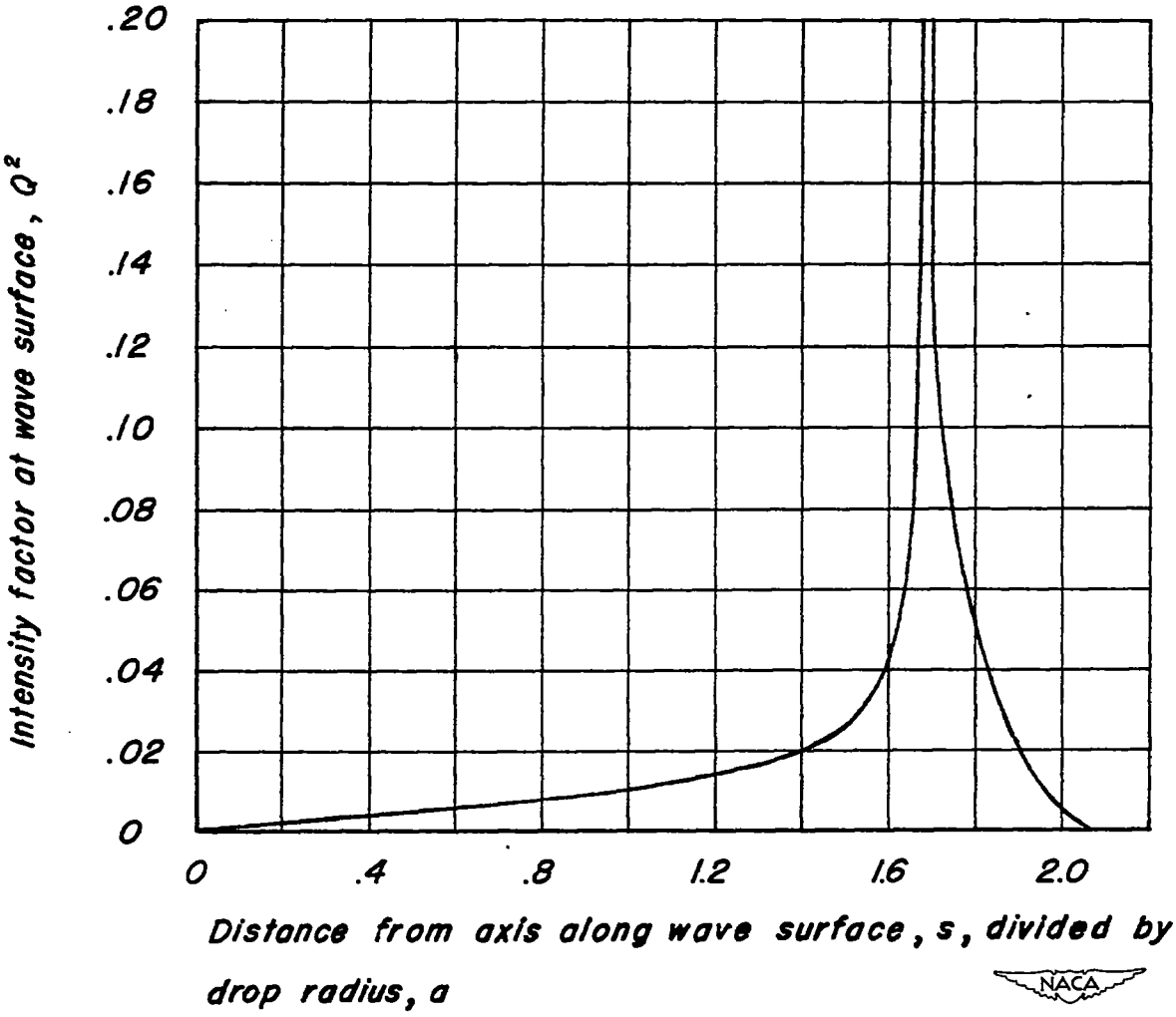

Figure 16.- Intensity distribution at the constant-phase surface.

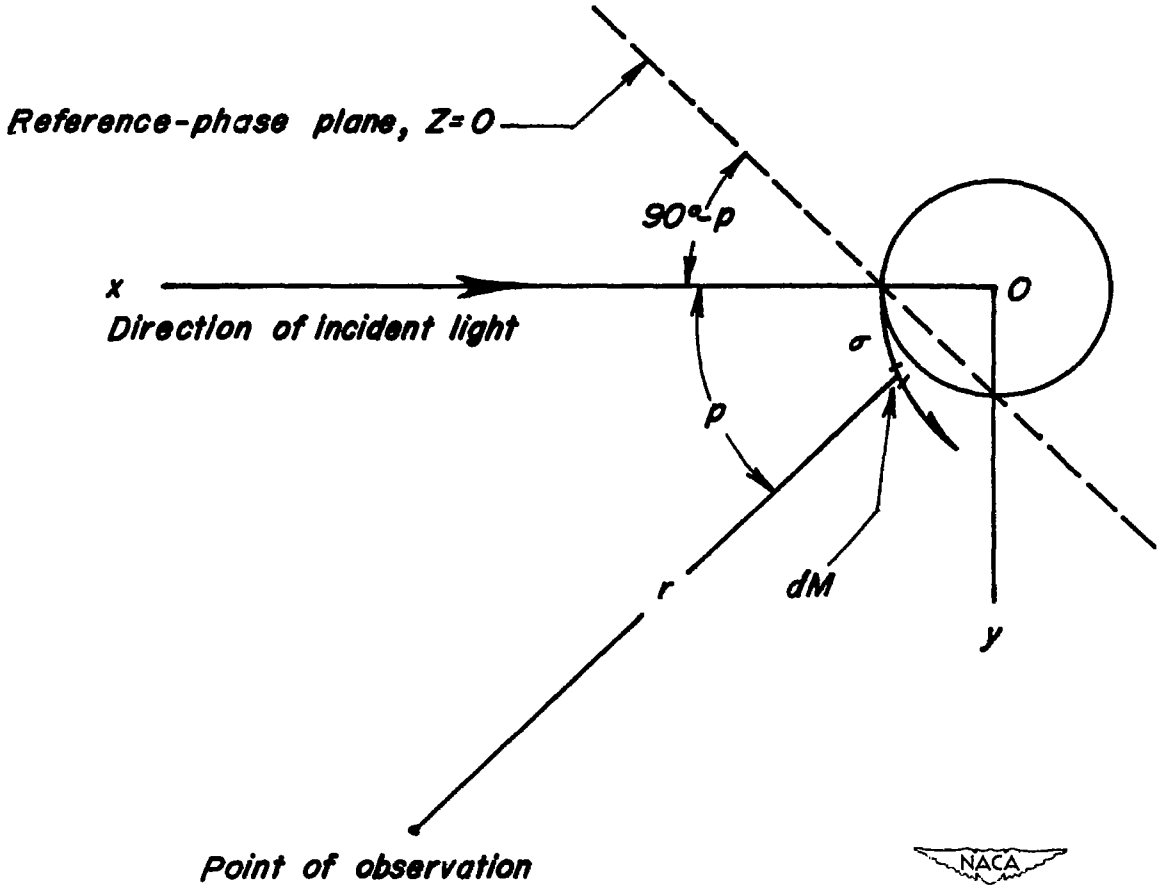

Figure 17.- Diagram showing definition of angle of viewing, p, and location of the reference-phase plane, Z=0.